POLITECNICO DI TORINO

Master's Degree in Civil Engineering

Performance Base Design of the Messina Strait Bridge

Numerical Analysis and Experimental Setup of a Scaled Model

Supervisors:
Prof. Gian Paolo Cimellaro
Prof. Farhad Ansari

Student:
Salvatore Marrocco

Academic Year: 2024/2025

Abstract

The objective of this thesis is related to the design of a scaled model of the Messina Strait Bridge and analyze its behavior when subjected to ground motion. By using similitude theory, a scaled model was built in the laboratory of the University of Chicago using a scale factor of 1/265, according to laboratory dimension. In order to simulate different soil conditions, a spring-box system was designed and implemented and by changing the spring stiffness three different soils were studied, in particular a soft soil, a medium soil and a hard soil having respectively a stiffness of 4 N/mm, 20 N/mm and 200 N/mm. Additionally, a finite element model generated on Midas Civil was used to perform a numerical analysis useful to identify the best sensors placement, including Fiber Bragg Grating (FBG) and Linear Variable Differential Transformers (LVDT). The bridge's behavior in damaged and undamaged configuration was investigated on numerical analysis and its damaged behavior under seismic motion will be investigated on experimental analysis, which is currently pending, as the software Midas Civil does not support the application of ground motions in this specific configuration. Despite this limitation, numerical results revealed that damage in suspenders lead to a highly localized effect and in particular only suspender adjacent to the broken one are affected and subjected to a substantial increase in tension, while those farther away are minimally involved. As regards vertical displacements, similar results are observed, as increse in displacement is concentrated only in the area surrounding the damaged suspender and the recorded tension in the main cable remains almost unchanged. It was also observed that suspenders located on the opposite side of the bridge from the damage location were not influenced by the failure. The illustrated results are obtained by performing DCR analysis that also showed that shorter suspenders tend to exhibit higher DCR values, revealing a lower safety margins and a need for immediate replacement in case of damage. Furthermore, the designed spring-box system proved its effectiveness in replicating different soil condition and revealed the importance of modelling the soil-structure interaction (SSI), when developing a FEM model, to have reliable results. Neglecting SSI may lead to a significant underestimation of the structural response. Finally, two ground motions were applied on the numerical model in the undamaged configuration, in particular a near-fault ground motion and far-fault ground motion have been selected, showing how the near-fault combined with softer foundation stiffness lead to larger displacements compared to the other cases. This results revealed the importance of the SSI in the seismic performance assessment of a bridge model. These findings lay the foundation for further experimental and numerical investigations related to the seismic behavior of suspension bridges.

Acknowledgments

At the end of the university journey, I feel I have to thank people who have made this experience meaningful and enriching. First of all, I wish to express my graditude to my supervisors, Professor Gian Paolo Cimellaro and Professor Farhad Ansari for giving me the extraordinary opportunity to carry out my thesis project at the University of Chicago. A hearthfelt thank you goes to my family, my mother, my father and my sister Francesca who have always been by my side and for always supporting me. All your sacrifices and your constant presence have been essential ingredients for achieving any of my goals. Without your love and encouragment, reaching this achievement would not have been possible. Lastly, I want to extend my gratitude to all my friends and colleagues who have shared this journey with me. Together we faced challenges and celebreted victories creating memories that will stay with me forever. Your presence transformed my time in Turin in an unforgettable chapter of my life. I will carry each of you with me, always.

Contents

List of Tables

List of Figures

Chapter 1

Introduction

Suspension Bridge is probably one of the first type of bridges ever built by primitive by using ropes, between rocks, to cross bodies of water such as straits and rivers. In moder age, the span length of suspension bridges is increased a lot thanks to the improvements in construction technologies and development of elastic theory and deflection theory. Nowadays the longest suspension bridge is the Cannakkale Bridge in turkey completed in 2022 with a main span of 2023 m. The Messina Strait Bridge would be the longest suspension bridge ever realized, it is characterized by an innovative aerodynamic design for the deck and a main span of 3300 m. Suspension bridges are structure with high flexibility and it is well known that this characteristic is related to the adoption of new high-strength and light weight materials. It is a structure designed to have a very long nominal life and for this reason, given the high distance between the two anchors, it is very likely to be subjected to tectonic shifts during its lifetime and this effect could be amplified in bridges crossing active faults. Furthermore, relative displacements between the anchors of a suspension bridge could also occur during an earthquake because of very long distance between them, even though, thanks to their high natural period, they are not very sensitive to seismic actions. This effect could lead to high damage in case in which strong earthquakes causes large shifts [7]. The dynamic response is influenced not only by the seismic input but also by the interaction between the structure and the soil, identified as Soil-Structure Interaction (SSI). Understanding and accurately modeling this aspect is very important for the design and safety assessment of suspension bridges in seismic zones [17]. This thesis focuses on the creation and designing of a scaled model of the Messina Strait bridge in order to perform seismic analysis, by applying gound motions, in different configurations. The scaled model was built in the laboratory of University of Chicago with a scale factor of 1/265, according to the laboratory size, and it was ewuipped by FBG and LVDT sensors to record the structural response. The soil simulation has been conducted by designing a specific spring-box system allowing the representation of three soil conditions, in particular soft soil, medium soil and hard soil configuration. One other important aspect of this research is to study the bridge's behavior when subjected to damage in the suspenders. Suspenders are vertical cables used in suspension bridge to tranfer the load from the bridge's deck to the main cable. Damage or failure of one or more suspenders can lead to significant changes in internal force distribution and deformation patterns [19]. The software Midas Civil was used to create a finite element model of the scaled bridge and to study its behavior in both damaged and undamaged configuration under different scenarios. Given that, software Midas Civil does not support the analysis process in damaged condition, results will be studied and validated directly on

the experiment, which is still waiting to be completed. Despite this limitation, numerical analysis has been conducted in a static scenario and was useful to identify the best sensors placement. Numerical results showed that damage in the cable is highly localized and that only suspenders in immediate vicinity of the fractured one are subject to an increase in tension, while those farther are not affected. The same results are also recorded for the vertical displacements showing an increase only in proximity of suspender loss, while the main cable tension is almost unchanged. The illustrated results are obtained by numerical simulation analyzing the Demand to Capacity ratio (DCR) [19] and showing also how shorter suspenders record an higher DCR value indicating that are more subjected to fracture and are more vulnerable. Lastly, it was observed that the failure of one suspender has no effect on the bridge's opposite side, confirming the localized nature of the damage. As previously mentioned, the seismic behavior has been analyzed under different soil conditions, simulated with the spring box system, showing the important role of modelling the SSI when a bridge model is realized. Results show that neglecting the SSI can lead to an underestimation of the bridge's structural response compromising the accuracy of the results. Furthermore, two earthquake ground motions were selected, a near-fault and far-fault, to compare the bridge's behavior under two different seismic excitations. Both records were from the 2009 L'Aquila earthquake, with one from the AQK station, located directly on the fault rupture, and the other from the MTR station, approximately 16 km away from the fault rupture. These ground motions were scaled according to similarity laws to match the model requirements [13]. The results showed that softer soil conditions, especially when coupled with near-fault motions, produce the largest mid-span displacements as also confirmed in the following research [17]. To monitor the response, the following sensors are used:

- *FBG sensors* are positioned on the critical suspenders, SUS58 and SUS60, adjacent to the damaged SUS59, and SUS06 near the tower, which has the highest tension, to measure tensile forces.
- *LVDT sensors* are placed at the top of the tower and at mid-span to measure horizontal displacements.
- *Accelerometers* are used to record the dynamic response during seismic motion.
- *Shakers*, are controlled via LabVIEW, applied the ground motions to the base of the structure, reproducing the desired seismic events.

The research presents the design of the scaled model and its construction phase in the laboratory, with particular attention on numerical analysis useful for the experimental setup, and preliminary numerical findings to study bridge's behavior under different scenarios in both damaged and undamaged configurations. The results have the goal to improve the understanding of the bridge's behavior under ground motion considering the soil structure interaction and damaged configurations.

Chapter 2

State of the Art

A bridge is a structure built for carrying the road traffic or moving loads used to avoid physical obstacles without closing the way underneath such as a valley, a road or a body of water. [4] Other type of obstacles can be rivers, railway, sea channels and costructions such us bridges themselves and buildings. Design of bridges requires a complex study and depends on the type and the function of the needed bridge, the used material to built it and the type of the terrain where is constructed or anchored. [4] [11] The difference in bridges type depends on the used deck types and various bridge properties. Main elements which compose a bridge are superstructure, substructure, bearings, foundations.

- Superstructure
  - the superstructure is in general the part of the structure above the bearings which supports traffic and includes deck, slab and girders. The deck is the part of the bridge which suports the traffic load and transmit them to the substructures. As shown in figure 2.1. [4] [11]
- Substructure
  - the substructure is the part of the bridge below the bearings, such us piers and abutments. It is used for supporting the bridge superstructures and to transfer all the load through the foundations to the ground. As shown in figure 2.1 and 2.2. [4] [11]
- Bearings
  - The bearings are necessary components for a bridge used to transfer the load from the superstructures to the substructures and to create a connection between them. Bearings allow to have controlled relative displacement due to temperature and due to earthquake, reducing the stress involved.
- Foundations
  - Foundations are elements used to transfer the load from the substructure to the ground. The type of foundation adopted depend on the geotechnical properties of the ground. [11].

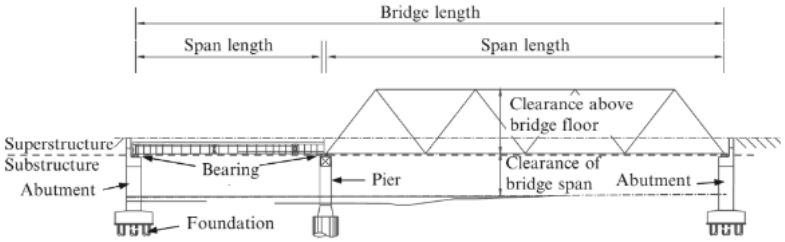

Figure 2.1: General Terminology of bridges: longitudinal direction

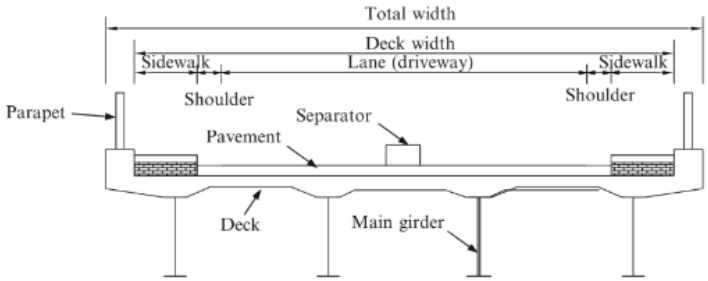

Figure 2.2: General Terminology of bridges: cross section

2.1 Classification of Bridges

Bridges can be classified in different ways and the classifications depend on the type of bridge'superstructures and bridge's substructures according to the following charachteristics:

- Construction materials
- Span length
- Position
- Span types
- Deck locations
- Usage
- Geometrical shape
- Structural form

2.1.1 Classification according to construction materials

Bridges can be named according to the type of material in which superstructures are built such as steel, timber, concrete, stone, alluminium and composite materials. Usually a bridge is formed by the combination of more materials. [4] [11]

2.1.2 Classification according to Span Length

Generally a bridge is classificated according to the span length as short span, medium span and long span bridges. The span classification of the bridges is proposed by Taly (1967) in the following way:

Culverts	$L \leq 6m$
Short-span bridges	$6m < L \leq 38m$
Medium-span bridges	$38m < L \leq 125m$
Long-span bridges	$L > 125m$

Table 2.1: Classification according to span length

Bridge span length classification is made for sake of description only because for certain type of bridges are suitable only certain type of span length. [4] [11]

2.1.3 Classification according to Position

Is a particular type of bridge called movable bridge in which the deck can be moved, most often powered by electricity, to allow usually the passage of boats or barges. This type of bridge are usually characterized by high maintenence costs. The main type are bascule bridges, swing bridges and lift bridges. [4] [11]

Bascule bridges

In this type of bridge the main girders are lifted together with the deck through a hinge in the span ends.

Swing bridges

In the swing bridges both deck and girders are hinged about a vertical support in order to allow the traffic to cross. In the case of very small swing bridges is possible to have the hinge only in one end and the opening is like a gate.

Lift bridges

The lift bridge is equipped by gantries both at the piers and end of the span. The girders are lifted up by a hydraulic system to allow the free passage of the ship.

2.1.4 Classification according to Span Type

Bridges can be classified according to their span type in simply supported bridge, continuous bridge and cantilever bridge. [4] [11]

Simply Supported Bridges

For a simply supported bridge, the elements are simply supported at both ends, therefore are statically determinate structures. The whole length is usually divided in individual short span. As shown in figure 2.3 [11].

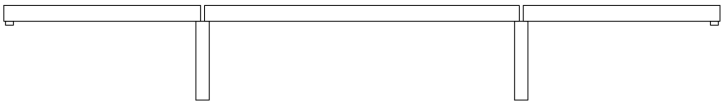

Figure 2.3: Simply Supported Bridge

Continuous Bridge

The continuous bridge has a continuous span over the all supports and it is a statically indeterminate structure. In this type of bridge the bending moment is smaller than the simply supported bridge because it does not have the rise of negative bending moment the support proximity. They are characterized by higher stiffner ratios, reduced deflections and less vibration. As shown in figure 2.4 [11].

Figure 2.4: Continuous Bridge

Cantilever Bridge

In a cantilever bridge all the structure is composed by cantilever beams. This type of bridges have a lot of advantages respect the simply supported bridge and the continuous bridge and they are suitable for foundation with uneven settlement. Furthermore, cantilever bridge has a larger span capacity. As shown in figure 2.5 [11].

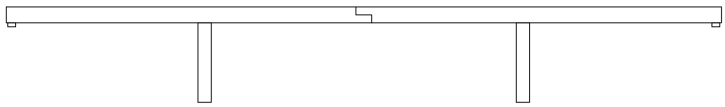

Figure 2.5: Cantilever Bridge

2.1.5 Classification according to Deck Location

This type of classification depends on the relative location between the deck and the load carrying structure and it is divided in deck bridges, through bridges, half-through bridges.

- *Deck bridge* is the case in which the deck is placed on the top of the main structure.
- *Through bridge* is the case in which the deck is placed on the bottom of the main structure.
- *Half-through bridge* is the case in which the deck is placed in the middle of the main structure.

2.1.6 Classification according to Geometric Shape

The bridge can be classified by its geometric shape as straight bridge, skew bridge and curved bridge. [11].

- *Straight bridge* is the case in which the axis follow a straight line.

- *Skew bridge* is used when the geometry can not allow a straight deck axis. According to AASHTO Bridge Design a skew angle lower than 15° can be neglected and for angles larger than 30° the effect should be considered in the analysis. This type of bridge tends to rotate under seismic loading.

- *Curved bridge* is the most difficult both in design and construction and it is used only when the bridge need to be curved for geographical purpose.

2.1.7 Classification according to Usage

The usage classification is related to the utility of the bridge and is possible to identify the highway bridge that are designed to carry vehicle load and pedestrian load; railway bridge that are designed to carry mainly railroad traffic load; pedestrian bridge that is designed to carry pedestrian, cyclist and animal load. There are also other type of bridge designed to carry non-vehicular load as aqueduct bridge, pipeline bridge and airport runway bridge.

2.1.8 Classification according to Structural Form

A bridge can also be classified according to its structural form and different type of bridges have different type of load path and are suitable in different situations. The type of bridges are beam bridge, rigid-frame bridge, truss bridge, arch bridge, cable-stayed bridge and suspension bridge.[11] [4].

Beam Bridge

The beam bridges are the oldest and simplest bridges type, hence they are the most common and inexpensive existing, consisting of vertical piers and horizontal beams supported at each end by piers or abutments. When it is subject to positive bending moment the bottom fibers are streched and the upper fibers are in compression, therefore for this typology of bridge only material with both resistance in tension and compression are allowed. Nowadays the most used materials are either steel or reinforced concrete with prestressing. This type of bridge are classified into slab bridges, when there is the span without supports below the deck, beam bridges, when there is only the longitudinal supports below the deck, and girder bridges, when there are both logitudinal and transversal structural members under the deck.

Rigid-Frame Bridge

The rigid-frame bridge is composed of a superstructure supported on vertical or monolithic legs and furthermore, superstructure and substructure are rigidly connected. The rigid connection between superstructure and substructure transfer bending moment, shear and axial force. Given that, for this type of bridges, the moments at the center of the deck are smaller than the corresponding moment of the simply supported bridge, a much smaller cross section at mid-span can be used.

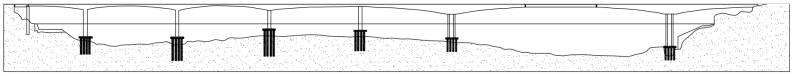

Figure 2.6: Rigid-Frame Bridge

Truss Bridge

Truss bridge consists of an assembly of triangles. The laod-bearing superstructure is composed of truss elements. To have a easier calculation, the truss are considered as pinned connection between adjacent truss members. Generally the truss elements are chords, verticals, and diagonals and they respond only either tension or compression.

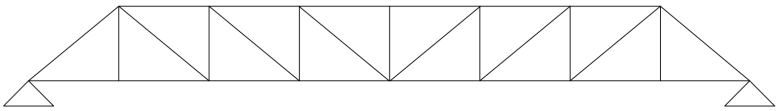

Figure 2.7: Truss Bridge

Arch Bridge

Arch bridge tranfer the weight into horizontal thrust restrained into the abutments at each side. They are made of more hinges and has a great natural strength. The arch carry bending moment, axial force and shear force and given that is a statically indeterminate structure, the internal forces will occur due to temperature variations and settlements of supports.

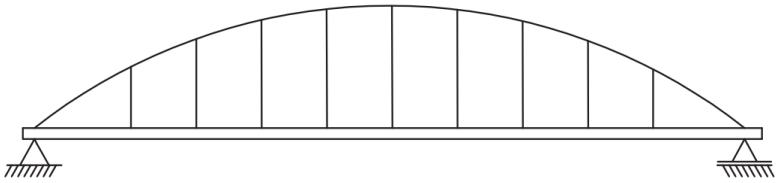

Figure 2.8: Arch Bridge

Cable-Stayed Bridge

The cable-stayed bridge is composed by several points in each span between the towers supported by inclined cables. It is formed by main towers, main girders and cable-stays. It is a statically indeterminate structure and it is also highly efficient in the use of material because its structural members works in either tension or compression. Cable-stayed bridge are able to reach great span length up to 1000 m.

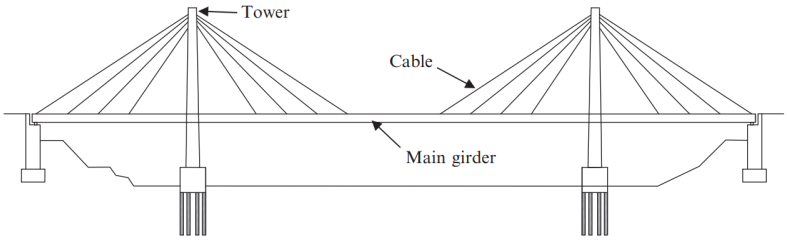

Figure 2.9: Cable-Stayed Bridge

Suspension Bridge

Suspension bridge is generally composed by a girder suspended by suspension cables which pass over the tower thanks to saddle and then achored to big anchorage blocks. Suspension bridge is formed by towers, main cables, main girder, hangers and anchorage blocks. The forces in suspension bridges are tension in the cables and compression in the towers. The deck is usually a box girder and it is supported by the hangers in tension. The load path consists in the transfer of the weight from the deck, through the suspenders, to the main cable, that transfer the load to towers and anchorage blocks and then finally goes to the ground. Suspension bridge are used to cover long span and they can be realized for span up to 3 km and larger [11].

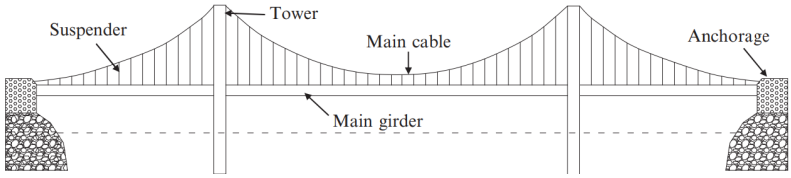

Figure 2.10: Suspension Bridge

2.2 Suspension Bridges

A suspension bridge is a particular type of bridge in which the deck is held by hangers connected to main cable. The main components of the suspension bridges are the stiffening girders or trusses, the main cable, the main towers, the suspenders (hangers) and the anchorage blocks. The main cable pass over the towers and are fixed to the anchorage blocks and the hungers carry the deck weight and the traffic load transferring all the load through the main cables, to the main towers and ground. Therefore the element that mostly carry the load is the main cable, made of high-strength steel and works in compression only. In this way is possible to amortize the deck weight and to realize larger span [11]. The stiffening girder is the deck composed of a longitudinal stiffening system used to support and to spread the vertical live load. The main towers supports main cables at the appropriate height taking into account the required sag and clearance and transfer the laod to the foundations. The anchorage block is a concrete block in which the main cables are fixed and it is used to avoid horizontal displacements of the structural system [11]. The hangers are connected to the deck and are used to transfer the live load to the main cable. All the described elements are showned in figure 2.11.

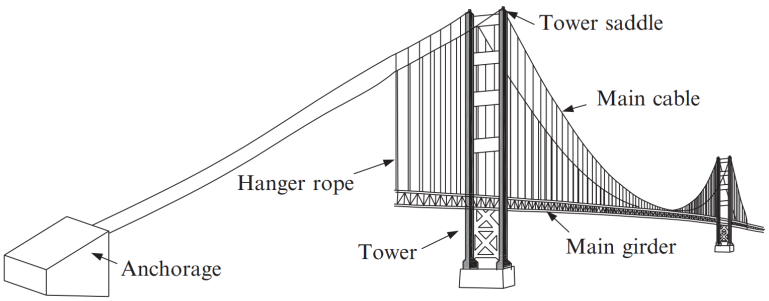

Figure 2.11: Suspension Bridge Components

For the construction of a suspension bridge, is necessary to continue in an appropriate phase in order to allow a favorable transmission of dead load. In general the anchorage blocks, the towers, the main cables and suspenders, and the deck, are erected in sequence [11]. For the erection of the towers are used cranes or floating cranes in the case of off-shore towers. For the erection of the deck two procedure can be followed depending on the fact wheter that the deck is used for externally anchored or self-anchored suspension bridges. In the case of self-anchored suspension bridge is necessary the use of falsework during the construction phase. In the case of externally anchored suspension bridge the use of falsework is not required and the used erection phase are either deck erection starting at the mid-span or deck erection starting at the towers [11].
In the first case the deck is lifted using cranes and it is anchored thanks to the hangers to the main cable and then the adjacent girders are connected through temporary joints. In the meanwhile, the erection of the sidespan can start simultaneously to avoid huge deflection, reducing the ending moment at the towers and set the cable shape. 2.12

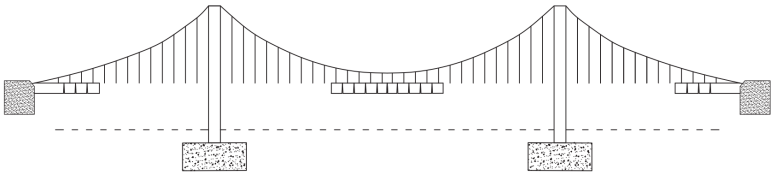

Figure 2.12: Erection Sequence from Mid-Span

For the second case the deck is erected in proximity of the towers and continue until the mid-span is reached. 2.13

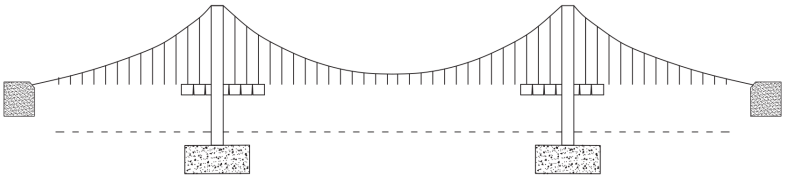

Figure 2.13: Erection sequence from Tower

2.2.1 Suspension Bridge Classification

There are different ways to classify a suspension bridge [11]. It can be classified according to:

Span Numbers

This classification is related to numbers of the span, therefore can be classified in single-span bridge, two-span bridge and three-span bridge as is shown in the following figures 2.14, 2.15, 2.16.

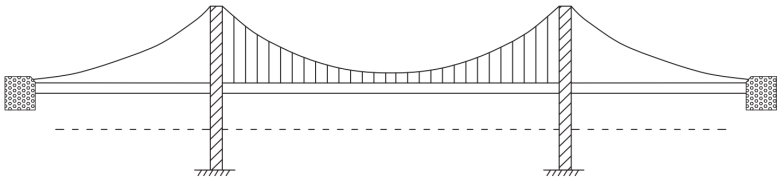

Figure 2.14: Single-Span Suspension Bridge

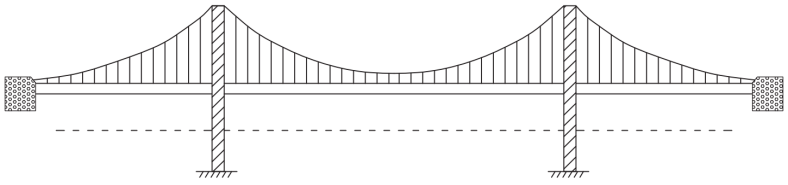

Figure 2.15: Two-Span Suspension Bridge

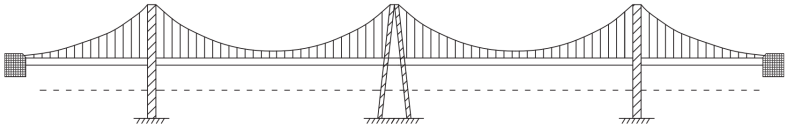

Figure 2.16: Three-Span Suspension Bridge

Stiffening Girders

The classification related to the stiffening girders include wheter the bridge is composed by two-hinge deck or continuous deck. The two-hinge type is used for highway bridge 2.17, instead the continuous type is used in the case in which there is a combination of highway and railway to guaratee the smooth passage of the train 2.18.

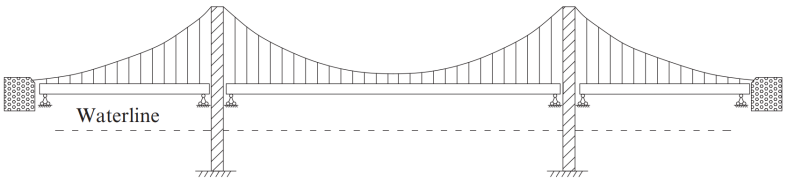

Figure 2.17: Two-Hinge Stiffening Girder

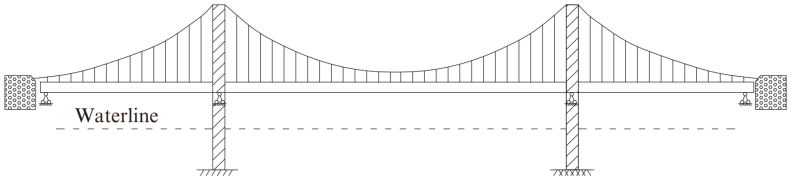

Figure 2.18: Continuous Stiffening Girder

Suspenders

The hangers are designed to support the deck and they can be vertical or diagonal. The most common suspenders are the vertical one 2.19 but sometimes the diagonal suspenders are used in order to increase the damping of the structure and therefore the seismic performance 2.20. To obtain furher high stiffness, combination of them can be used as shown in the figure 2.21.

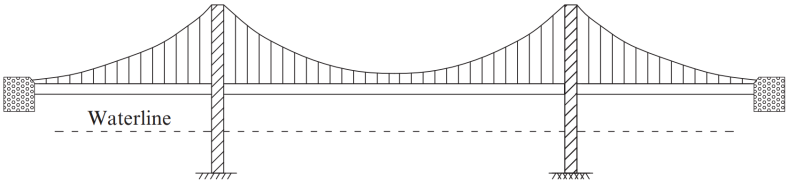

Figure 2.19: Vertical Suspenders

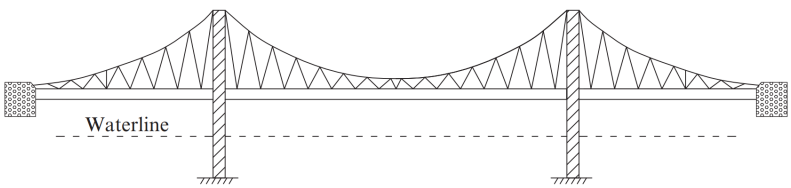

Figure 2.20: Diagonal Suspenders

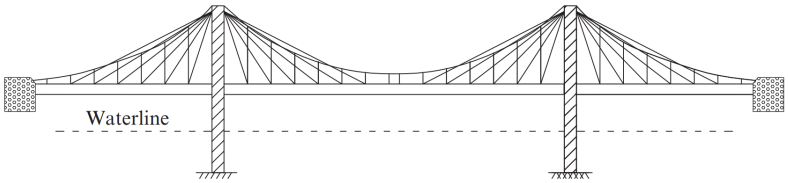

Figure 2.21: Combination of both Diagonal and Vertical Suspenders

Anchoring Conditions

The classification related to anchoring condition is divided in two categories. The first one is called externally anchored bridge 2.22 that is the case in which the bridge has the need of anchorage blocks to sustain the tensile force of the main cable; the second category is called self-anchored suspension bridge and in this case there is no need of anchorage blocks and the main cable are directly connected to the deck 2.23.

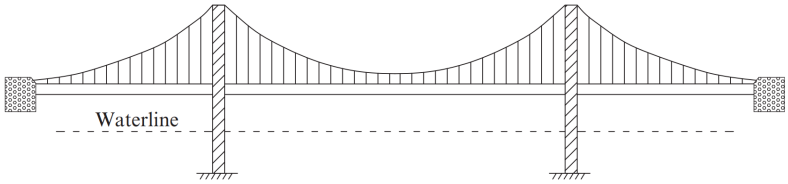

Figure 2.22: Externally Anchored Suspension Bridge

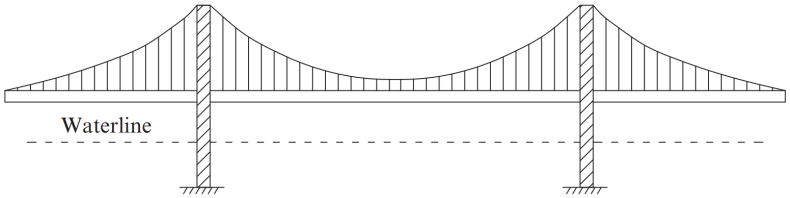

Figure 2.23: Self-Anchored Suspension Bridge

2.2.2 Suspension Bridge Configuration

In the study of a suspension bridge, is important to introduce and to study the Sag and the Sag Ratio. The Sag is denoted as (f) and represent the vertical distance of the main cable in the main span of the bridge. The Sag is used to control the length and the stability of the suspension bridge and usually is chosen as a value between 1/8 and 1/12. The Sag Ratio is defined as the ratio between the sag and the length of the bridge, denoted as $n = f/L$, and is used to identify the shape and the type of stress that occurs in the bridge. If the sag ratio is low, the bridge has more vertical stability but the stresses in the cables are very high therefore strong anchorages are required; in the case in which the sag ratio is high, the stresses in the cables are lower but is necessary to increase the height of the towers. In the following figure 2.24 the geometrical shape is shown in which the x-axis identify the horizontal direction and the y-axis identify the cable deflection [11].

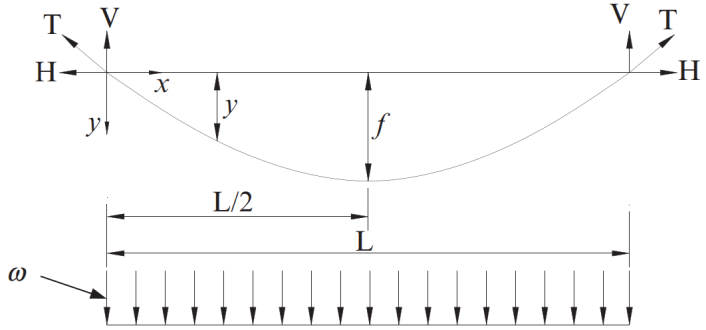

Figure 2.24: Shape of the Main Cable

The bending moment in the cable is equal to zero and it is calculated as:

$$M = M_0 - Hd_\gamma = 0 \tag{2.1}$$

and considering ω as dead weight, the terms of the equation (2.1) are:

$$M_0 = \frac{\omega L^2}{8} \tag{2.2}$$

$$H = \frac{\omega L^2}{8f} \tag{2.3}$$

Defining as M_0 the bending moment at the span center and H the horizontal force. The geometrical shape equation is determined as:

$$\gamma = \frac{4fx}{L^2}(L - x) \tag{2.4}$$

The main components of a suspension bridge are main towers, cables, stiffening girders and anchorages.

Main Towers

The main towers are classified in three different types according to the length and the type of suspension bridge. They are divided in rigid, flexible and locking types. The rigid towers are used for multispan bridge when high stiffness is required; the flexible towers are mostly used in long-span bridges; locking towers are used in a case of very short span suspension bridges [11].

Cables

The cables used in a suspension bridge can be of different types. In general for the main cables are used either cold drawn or galvanized steel wires and each strand is grouped into a circular shape to form one primary cable. For the hangers (suspenders) can be used steel rods, steel bars, stranded wire ropes or parallel wire strands [11].

Stiffening Girders

The most used stiffening girders are I-girders, trusses and box girders. The disadvantage of the I-girders is related to the low aerodynamic stability. Nowadays trusses or box girders are most used and with this type of deck there is an increasing of both the stiffening and the bending moment due to temperature. In case of

a long-span bridge, the dead load is included in a big part of the carrying capacity of the bridge and therefore the increase of the deadload causes a decreasing in the capacity of the bridge to carry the live load. Hence, is necessary to decrease the dead weight to increase the carrying capacity of the live load by using thinner either trusses or box girders [11].

Anchorages

In the anchorage all the loads of the bridge are transferred and inside the anchorages the cable are spread in a large area to reduce local effects which can cause high local damages. The most used anchorages are of two types: gravity type and tunnel type as shown in figure 2.25a and in figure 2.25b respectively.

(a) Gravity Type (b) Tunnel Type

Figure 2.25: Anchorage Systems

The gravity types are constituted by a big concrete block and the carrying capacity depends on the self-mass in order to resist to tension induced by main cables. In the tunnel types the tension of the main cable is sent directly to the ground [11].

Chapter 3

Messina Strait Bridge

3.1 Definitive project

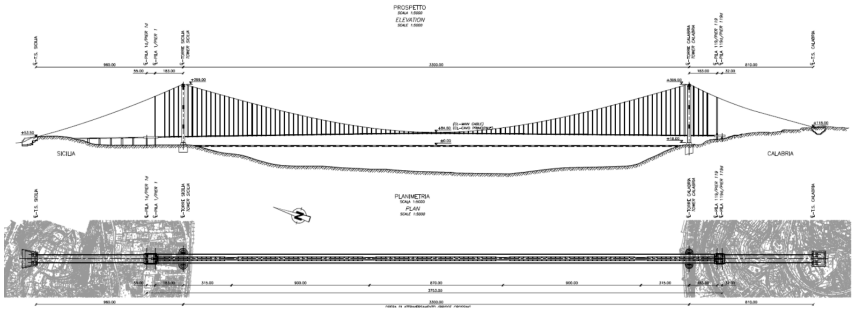

Figure 3.1: Messina Bridge

The Messina Strait bridge is the result of over 40 years of research and projects that were slowly improved in the time in order to achieve a high level of design characteristics. The chosen solution was selected to be a suspension bridge having the towers located on Calabria and Sicilia land. Regarding safety level, an extremely high return period is used both for SLS (serviceability limit state) set at 200 years and for external action as wind and earthquakes set at 2000 years. Between all the solutions was studied a type of solution in the shortest distance between Sicily and Calabria. An other important aspect is the sag ratio used to minimize the weight and stiffness of the main cable, and for the messina bridge a sag ratio of 1:11 was chosen. The project includes four traffic lanes for vehicles, two emergency lanes and two railway tracks. The deck is composed of three independent steel orthotropic box girders, one for each of the two roadways and one for the railway and all these box girders are connected between each other through steel beam spaced 30 meters. The deck is hold by suspenders connected to the cross beams and then are connected to the main cables. The main cables are big steel cables and are present three different diameters: a diameter of 1.16m on the leftside span, a diameter of 1.14m on the main span and a diameter of 1.15m on the rightside span. The main cable pass over the towers with a height of 399m over the sea level and end to the anchorage blocks. The towers have foundations made of prestressed reinforced concrete, supported by the underlying rock formations. As regards the effect of wind, the Messina Strait Bridge has been designed to remain open all the year without traffic interruptions. This is possible thanks to the adoption of special wind barriers that allow regular traffic flow even during strong winds.

As regards instead the seismicity zone, is possible to say that the suspension bridges are structure that generally are not very sensitive to earthquakes, thanks to their structural configuration which provide a kind of natural isolation resulting from the difference between the frequencies typical of seismic excitations, fraction of seconds, and the physical ability of the structure to vibrate, with periods of severals seconds or tens of seconds. The Messina Strait Bridge has been designed to withstand an "extreme" earthquake of 7.1 on the Richter scale (the maximum recorded in Italy), with the hypocenter located about 15 km from the bridge. In the design of the Messina Bridge, it was determined that in the event of a severe seismic event, the structures would remain intact (responding elastically), with performance exceeding the design specifications, which allow for partial damage in the case of a high-magnitude earthquake. The bridge would therefore have a reliability margin beyond the design threshold. The Strait area's seismic potential cannot generate earthquakes of significantly higher magnitude than those established for the design. Additionally, the infrastructure connecting the bridge to the mainland, such as viaducts and tunnels, is designed, following legal standards, using the most advanced seismic criteria [5]. The Strait of Messina is in a region of the Mediterranean basin characterized by high geodynamic activity in particular during the quaternary period and the last 700.000 years. During this time the western side of the Aspromonte range has seen an uplift of about 300 meters as indicated by the remains of the terraced landforms. From observations obtained by terraced landforms is possible to evaluate the average uplift rate that is about 1.2 mm per year. From a tectonic point of view, the Strait of Messina is set in a system of faults that define a structure similar to a tectonic rift or graben. Due to this dynamic aciv-ity there is the rise of energetic and destructive earthquake. Studies conducted in space geodesy indicate that Sicily and Calabria experience horizontal displacement of about 10 mm per year and even if both regions moves forward north, they tend to divert. However there is still not enough knowledge on the active faults responsible for these movements that caused some of the strongest earthquake through the history, such as the Vivenzio Earthquake in 1783 and another one in 1908. The Aspromonte fault has been identified as the surface of the earthquake's sismogenetic structure happened in 1783. This fault is still active and it produced several earthquake during the history with enough energy to produce surface ruptures. By observing the similarity between Aspromonte fault and Messina, Sant'Eufemia, Delianova and Arno fault has been deducted that these faults caused the last earthquake recorded between Catanzaro and Strait of Messina. [3] The geotechnical investigation conducted between the 1988 and 1992, with the geological and geophysical surveys for the preliminary design study, provided a detailed knowledge of the soil profile in the Strait of Messina area. About the sicily side, the current ground level at the sicilian tower site is approximately 4-5 meters above the sea level, with a slight slope towards the coast which is about 60-70 meters from the tower's foundation center. The seabed's slope in this area is about 13 degrees and the groundwater level roughly coincides with the sea level, around 0 meters above sea level [8]. In the sicily tower and calabria tower, we can find these different soil layer:

- *Coastal Deposit:* Sand and gravel with low fine content, and also in the lower part there is the presence of silty layers.

- *Messina Gravel:* The gravel and sand layers have a thickness of approximately 140 meters at the tower location and 200 meters at the anchor block vicinity.

- *Continental Deposit:* consists of alternating layers of silt or silt and sand, with gravel content.

- *Pezzo Conglomerate:* A soft rock composed of clasts of varying sizes within a silty matrix.

- *Crystalline bedrock:* Tectonised granite

In the following figures are reported the main geotechnical parameters for Sicily side (figure 3.2) and Calabria side (figure 3.3):

	profondità (metri sotto il livello del terreno)	Dr * (%)	K_0*	φ'_p (°)	φ'_{cv} (°)	K_h (m/s)	G_0 (MPa)
Depositi costieri	0÷68	80÷55	0.43÷0.47	44	(33÷35)÷(35÷37)	5×10^{-3}	50÷200
Strato di transizione	68÷84	55	0.47	42	35÷37	5×10^{-3}	350
Ghiaie di Messina	84÷210	55	0.47	42	35÷37	5×10^{-3}	2500

Figure 3.2: Summary of Main Mechanical Parameters from Geotechnical Characterization of Sicily Side

	depth (m bgl)	Dr * (%)	K_0*	φ'_p (°)	K_h (m/s)	G_0 (MPa)
Coastal Deposits	0÷15	80÷60	0.43÷0.47	44	2.6×10^{-3}	100
Altered Conglomerate	50	60	0.47	42	2.6×10^{-3}	350
Pezzo Conglomerate	>50	70	0.6÷0.9	40		700

Figure 3.3: Summary of Main Mechanical Parameters from Geotechnical Characterization of Calabria Side

3.1.1 Towers

The towers of the Messina Strait Bridge are entirely made of steel and they are composed by two metallic legs interconnected by three cross beams. The height of the tower is 399 m with a weight of 55000 tons. Each tower has two legs composed by 22 prefabricated elements and each element has an octagonal cross section 20x12m with a maximum height of 20 m and a weight of 1200 tons. The main elements are legs, cross beams, base anchorage and, with respect to the preliminary project, the tower's height was increased from 382.60 m to 399 m to compensate the increase in the deck weight. Tower legs and cross beams are plated steel box shaped cross sections that are stiffened longitudinally and transversally. The base anchorage includes base plates, post-tensioning anchorage tendons and tower legs anchorage stiffening. The towers are fabricated in steel grade S460 ML with the exceptions of the hot-rolled circular hollow sections including the cross beam internal bracing members and the tower base plate and base anchorage which are built using S355 ML structural steel. Tower's legs cross section is constant along all the height with a dimensions of 12 meters in the direction perpendicular to the bridge axis and 20 meters in the direction parallel to the bridge axis, as shown in figure 3.4.

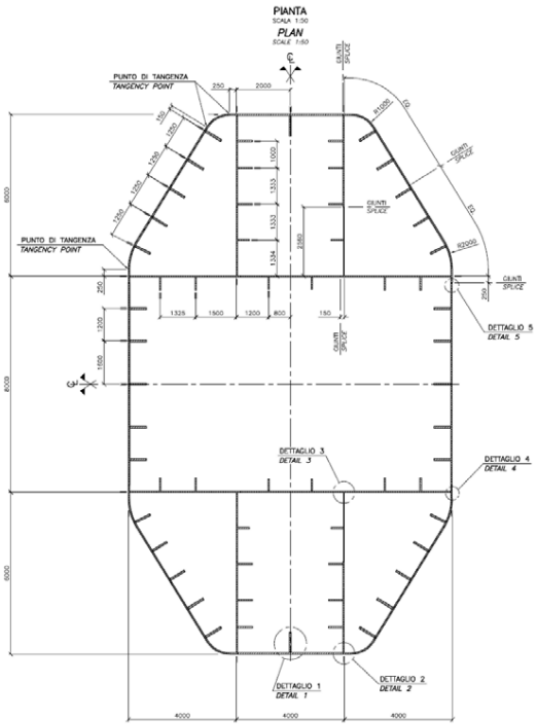

Figure 3.4: Tower Leg Cross Section

Furthermore the legs are inclined inwards at 1.929° with a centerline of 77.662 meters at the base and 52 meters at the top. In the original project the towers were designed to be straight and during the construction stage a tie-back force is introduced to gives an inclination in order to better balance the maximum stresses that acts on the main and side span face of the tower leg. There is the addition of cross beams along the height of the towers at an elevation of +125m, +250m, +375m respectively. In addition in each tower legs there are 8 TMD between a height of 230 meters and 260 meters to control the oscillations induced by the wind at a wind speed in a range of 40 m/s and 60 m/s. As

regards cross beams, each of them is 8 m wide and various in depth from 11.5 m in the centerline to 22 m, 20 m and 18 m at the tower leg face for cross beams 1,2,3 respectively. Each cross beam is prefabricated and erected and their role is to stabilize the tower leg from transversal buckling. Buckling phenomena of the tower causes additional moments and shears in the cross beams, figure 3.6. The tower base anchorage is composed by a multi-strands post tensioned anchorage tendons, the base plate and the local tower leg stiffening. The anchor bolts are replaced with post-tensioning tendons to reduce the quantity of foundation reinforcement [8].

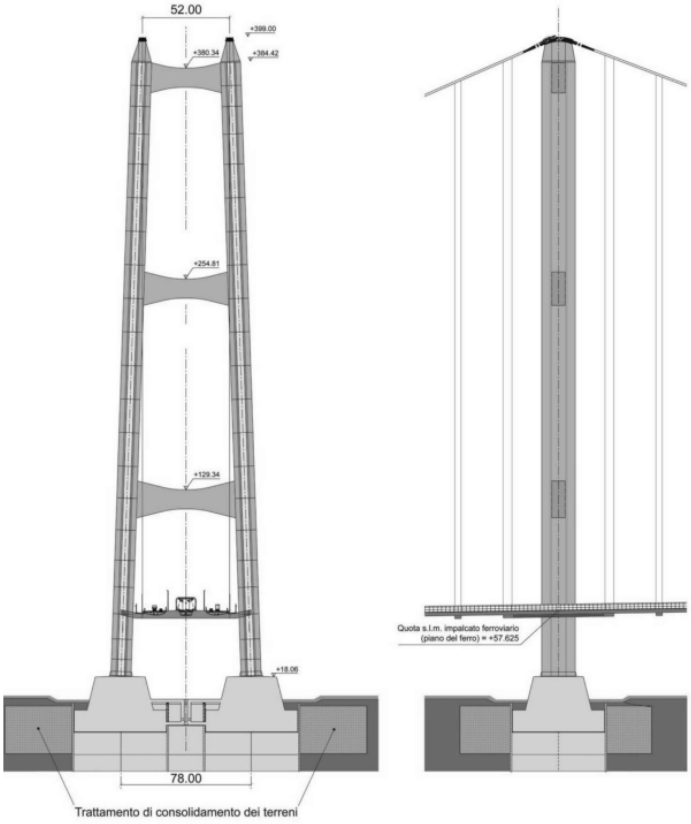

Figure 3.5: Messina Bridge's Towers

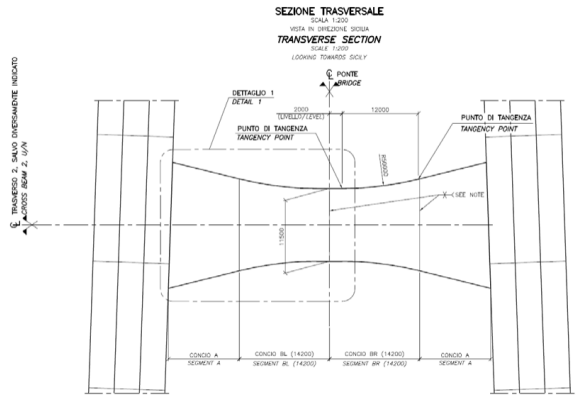

Figure 7-45: Cross beam 2 transverse elevation.

Figure 3.6: Cross Beams

3.1.2 Deck

The suspended deck of the Messina Bridge is 60 meters wide and entirely made of steel and it is formed by three independent longitudinal box girders, two for roadways and the central one for railways. The total lenght is of 3666 meters between the expansion joints and the distance between the towers is of 3300 meters. The extension of the deck beyond the tower is 183 meters until the terminal structure in Sicily and Calabria. Along the sides of the deck there are group of suspenders, called hangers, that suspend the deck from the main cable. The elevetion is of 76.8 meters on the sea level at the midpoint and 62.9 meters at the Calabria side and 51.6 meters at the Sicily side. The structure is a four-lane roadway platform with a railway in each direction. The deck cross section is designed in a aerodynamic way to optimize the airflow and in addition to ensure an optimal torsional rigidity. The cross beam are spaced of 30 meters and supported by the hangers, composed by a width of 4 meters and a varying height between 1.3 meters and 4.7 meters, made of steel mainly of type S355ML, with a total weight of about 18.10 tons per meter [8]. The main components are:

- *Roadway girders:* includes steel section stiffened by longitudinal stiffeners and transverse diaphragms. The box girder is connected to supporting cross girders and the box girders are completed by aerodynamics fairings.

- *Railway girders:* include steel sections stiffened by longitudinal stiffeners and transverse diaphragms and the railway girder sections are connected to the supporting cross girders.

- *Cross girders:* are placed every 30 meters and supported by the hangers. Cross girders support the railway and roadway girders and are formed as a closed box section of variable height.

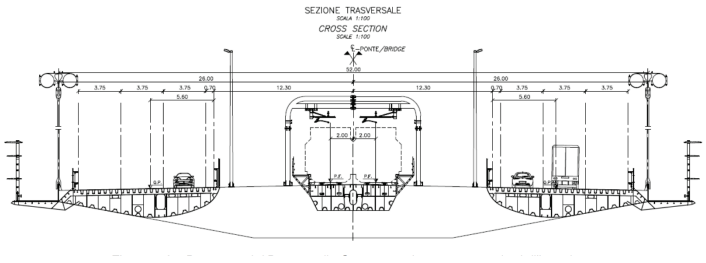

Figure 3.7: Deck Cross Section

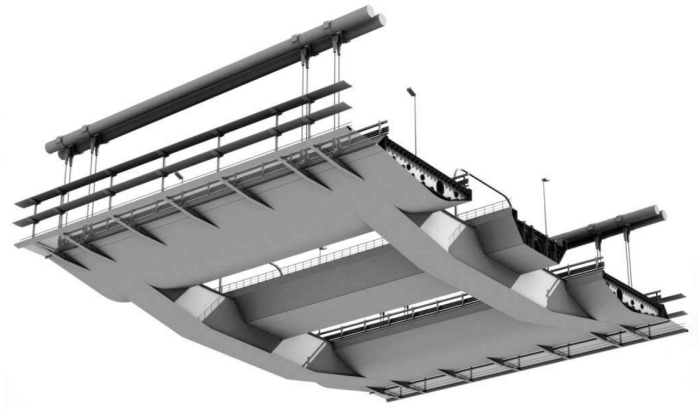

Figure 3.8: Render of the Deck

3.1.3 Foundations

The bridge interacts with the soil at the towers and at the two anchor blocks. The steel towers are connected to massive concrete foundations and both Sicily and Calabria towers have twin embedded cylindrical foundations with a diameter of 55 m and 48 m respectively. The two cylindrical foundations are connected thanks to a stiff box beam with a depth of 15 meters from the ground level. [6]

The foundation of the tower in Sicily comprises two massive circular concrete bases, each with a diameter of 55 meters and spaced 77.5 meters apart. These bases are connected by a cast-in-place, prestressed reinforced concrete box girder with dimensions of 15.50 meters in height and 18.00 meters in width, extending from -11 meters to +4.5 meters above sea level. The ground level at the foundation site is approximately 5 to 6 meters above sea level, sloping gently toward the coast, which is located about 50 to 60 meters from the center of the foundation. In front of the tower, the seabed descends at an incline of approximately 13 degrees. To reach the foundation depth of -15 meters above sea level, excavation is supported by circular diaphragm walls extending down to -45 meters above sea level. The diaphragm wall consists of reinforced concrete panels, each 1.00 meter thick and 3.00 meters wide, cast in place between +2.50 meters and -5.00 meters above sea level. In the figure 3.9 and in figure 3.10, are shown top view and lateral view of Sicily side foundation respectively. [8]

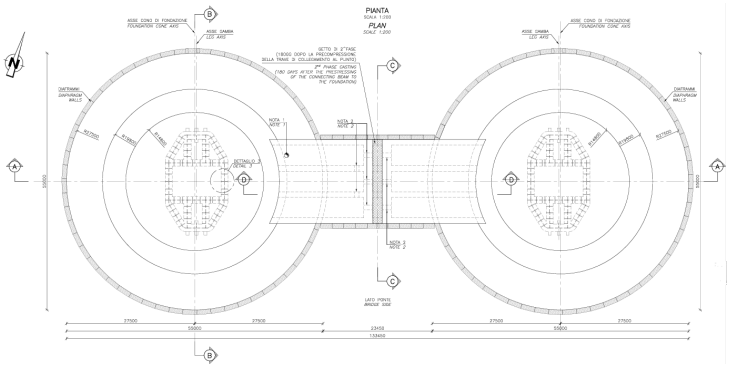

Figure 3.9: Sicily Tower Foundation: Plan View

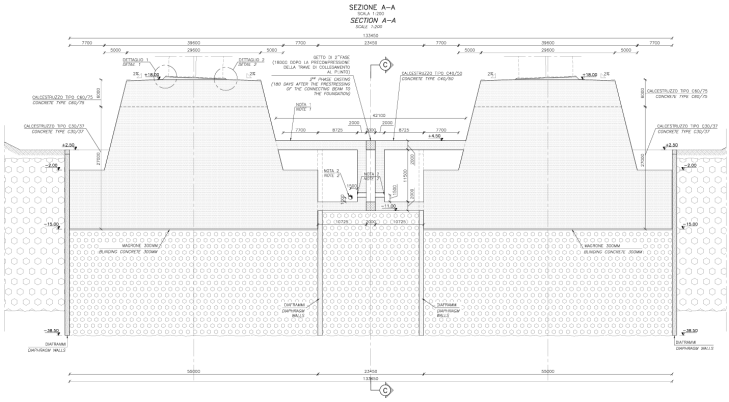

Figure 3.10: Sicily Tower Foundation: Lateral View

As regards the Calabria side, its foundation is formed by two large circular concrete bases, each with a diameter of 49 meters and spaced 78.45 meters apart from center to

center. These bases are linked by a prestressed reinforced concrete beam with a box-shaped profile, measuring 15.50 meters in height and 18.00 meters in width, constructed on-site between -11 meters and +4.5 meters above sea level. The ground at the foundation site is approximately 2.5 meters above sea level and slopes gently toward the coastline, which lies about 50 to 60 meters away from the center of the foundation. Ahead of the tower, the seabed inclines at an angle of roughly 26 degrees. To achieve the required foundation depth of -15 meters above sea level, the excavation is stabilized using circular diaphragm walls with varying depths, ranging from 47.5 meters to 62.5 meters. These walls are made of reinforced concrete panels, 1.00 meter thick and 3.00 meters wide, poured on-site from +2.50 meters down to -60 meters above sea level. [8] In the figure 3.11 and in figure 3.12, are shown top view and lateral view of Calabria side foundation respectively.

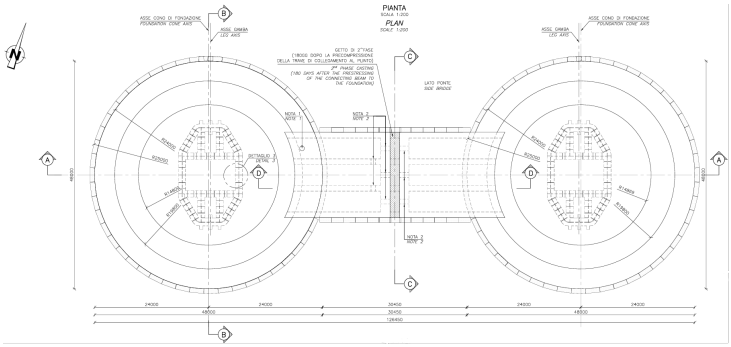

Figure 3.11: Sicily Tower Foundation: Plan View

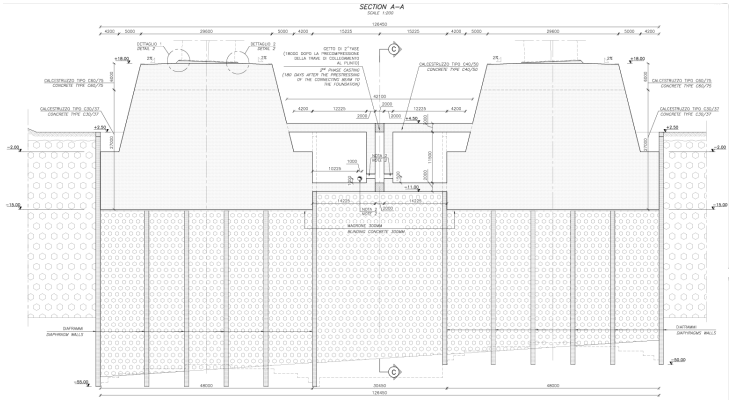

Figure 3.12: Sicily Tower Foundation: Lateral View

Below the foundations an extensive Jet-grouted area is planned composed by a thickness of 23 meters on the sicily side and a thickness varying from 11 m to 36 m on the calabria side. The lateral soil is also treated with jet-grouting for a distance of 60-40 meters from the foundation perimeter and having a thickness of about 33 meters on the Sicily side and a thickness varying from 21 meters to 40 meters on the Calabria side. The intervention involves the installation of jet-grouting columns with a finished diameter of 1600 mm, placed in an equilateral grid with a 1.20-meter spacing. While this configuration allows for comprehensive soil reinforcement, it falls short of ensuring ideal hydraulic continuity, especially when accounting for inevitable execution deviations, which can cause

the columns to deviate slightly from their intended vertical alignment. To improve sealing in the lower segment of the treated zone (the final 10 meters), the column diameter is increased to 1800 mm while retaining the 1.20-meter grid pattern. This modification ensures sufficient overlap between adjacent columns, even with vertical deviations up to 0.8-0.9%, which already represent stringent tolerances. The process uses a single borehole per column, employing two different sets of jetting parameters (adjusting the tool's upward movement speed) to create a wider diameter of 1800 mm at the bottom, transitioning to 1600 mm in the upper section. The depth of jet grouting differs between the Sicilian and Calabrian sides of the foundation. On the Sicilian side, the treatment follows a uniform depth profile, with jet grouting performed from -15.30 meters to -38.50 meters above sea level. Columns with a 1600 mm diameter are formed between -15.30 meters and -28.50 meters, while those from -28.50 meters to -38.50 meters have a diameter of 1800 mm. On the Calabrian side, the treatment depth exhibits greater variability due to the underlying geology. The Conglomerato di Pezzo bedrock is encountered at inconsistent depths along the route of the structure, from the coast to the inland section near the foundation. Above this layer there are recent coastal sediments, which are targeted for jet grouting, while the treatment stops once the borehole penetrates 0.50 meters into the substrate to ensure stability. The process starts at -15.30 meters above sea level, with treatment lengths ranging from at least 23.20 meters to roughly 50 meters. As with the Sicilian side, the lowest 10 meters of the treated zone, following the contact between sediments and bedrock, will use larger columns with a diameter of 1800 mm to create an effective hydraulic seal for the foundation. Between the base plug and the foundation level, only some of the columns will be constructed with a 1600 mm diameter, as the load-bearing role is also supported by the reinforced concrete diaphragm walls. The treated area encompasses about 55% of the total foundation footprint, using hexagonal array. The Jet-grouting has the purpose of inhibiting seismic liquefaction in the foundation soils. [8] [5]

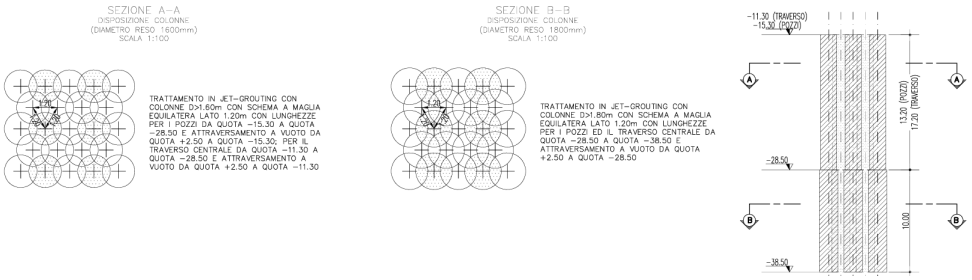

Figure 3.13: Jet-Grouting Treatment

3.1.4 Cable

The main elements to give suspension system are the main cables and they resist approximately to 67000 tons each. The main suspension system is composed of four main cable arranged in pairs and spaced 52 meters. These cable are composed of multi wire cable, in particular 349 wires, and after compaction the left side span cable has a diameter of 1.16 meters, the main span cable has a diameter of 1.14 meters and the right side span cable has a diameter of 1.15 meters as shown in figure 3.14. Their extension is about 3.370 meters across the main span and approximately of 1020 meters from the Sicily tower to the anchorage block and about 850 meters from the Calabria tower to the anchorage block achieving a total of 5240 meters between the two anchorage blocks. When installed, the bundle of wires that composes the main cable has a weight of 166800 tons and it is compacted in a circular shape and then treated with a surface coating to protect it from exposure damage such as corrosion and aggressive factors. The coating treatment is composed of three layer, one related to a viscous anti corrosive paste that fills the space between the wires, one related to a galvanized steel wire and a final paint layer. The two cables are connected every 30 meters with collars from which the hangers are attached, shown in figure 3.15. The distance between the two cable was increased from 1.75 meters to 2 meters to comply with the new design configuration [8].

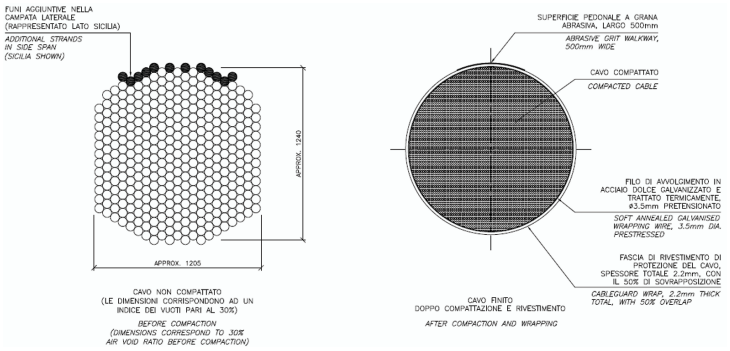

Figure 3.14: Main Cable Cross Section

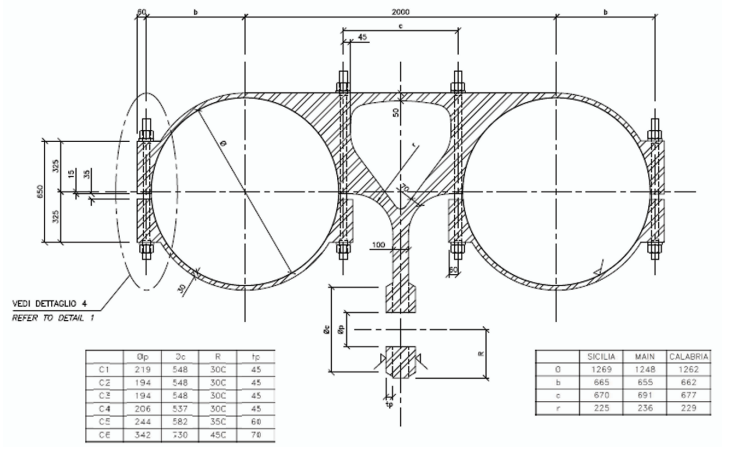

Figure 3.15: Collar Cross Section

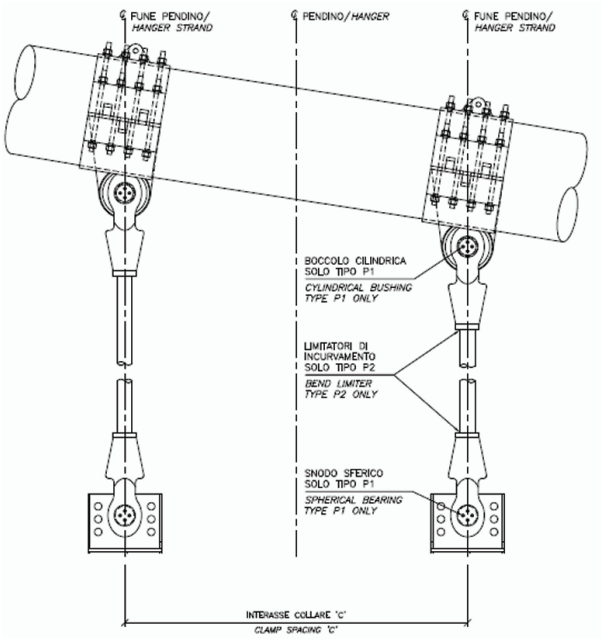

Figure 3.16: Hangers Lateral View

The hangers are the structural element used to transfer the load from the girder cross beam to the main cable. The typical hanger type will be Parallel Wire Strands (PWS) and it was selected for its high fatigue performance and increased breaking strength. Hangers diameters vary up to a maximum value of about 160 mm and the longest hanger close to the towers has a lenght of 300 meters and a weight of about 30 tons each. The hangers are placed every 30 meters in both sides of the girder and they are attached to the girder cross beams. A view of the hangers is shown in figure 3.16. Large diameter spherical bearings are used at both ends of the shorter hangers to provide and to allow rotations of the pinned joint around the the longitudinal axis in order to decrease the effects of the bending moment in the hangers due to relative longitudinal movement between the main cables and the deck [8] [5].

3.1.5 Anchorage Blocks

The anchorage blocks used as ending structure for the Calabria side and Sicily side are reinforced concrete structure with prismatic shape and designed to fit into the local morphology maximizing the contact surface with the ground. The total volume is approximately of 565000 m^3 but only the 17% of the volume is out the terrain and the main cables are connected to the block through anchorage plates. The blocks are designed to stand the tension from each pair of cables, approximately of 133000 tons. The two blocks in each side are different in morphology and in nature of soil on which they are located. The Sicily block is on slightly cemented gravel (Messina Gravel) and the Calabria block is on solid rock (Pezzo Conglomerate), this lead to an approximately volume of 328000 m^3 for the Sicily block and to 237000 m^3 for the Calabria Block. Inside the block anchorage there is a anchoring chamber for the main cable strands and each strand is anchored to the concrete block using a system of prestressing bars. In the figure 3.17, the resulting cables force acting on Sicily anchorage block are shown.

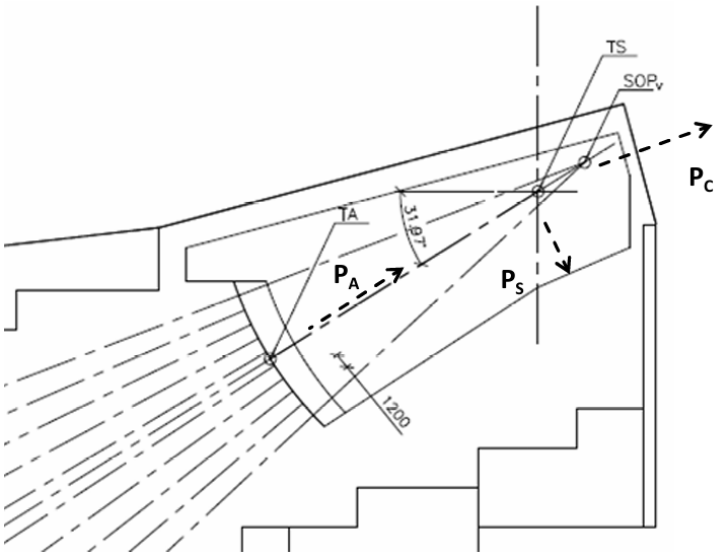

Figure 3.17: Resulting Cable Forces Acting on Sicilian Anchor Block

The roof of the anchor chamber has been designed using precast concrete elements that serve as formwork for a 0.3-meter-thick concrete slab placed on top. The overall height of the roof structure is restricted to 2 meters, leading to the selection of precast elements with a height of 1.7 meters. In the Sicilian anchor block, the roof is inclined at an angle of 15°, and it is planned that the precast elements will be positioned side by side, maintaining the same inclination. As regards the anchor chamber roof of the Calabria anchor block, it is inclined by 11° and also in this case it is assumed that the precast elements are placed besides each tower with the same inclination. As a result, the structure experiences a biaxial load condition. In the following figures are shown the geometric characteristics of the anchorage block for Sicily side [8].

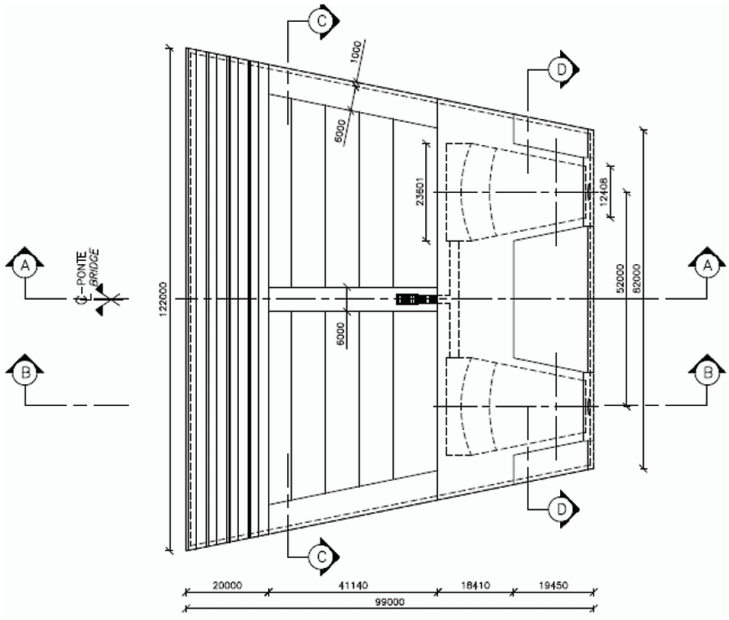

Figure 3.18: Anchorage Block Sicily Side: Top View

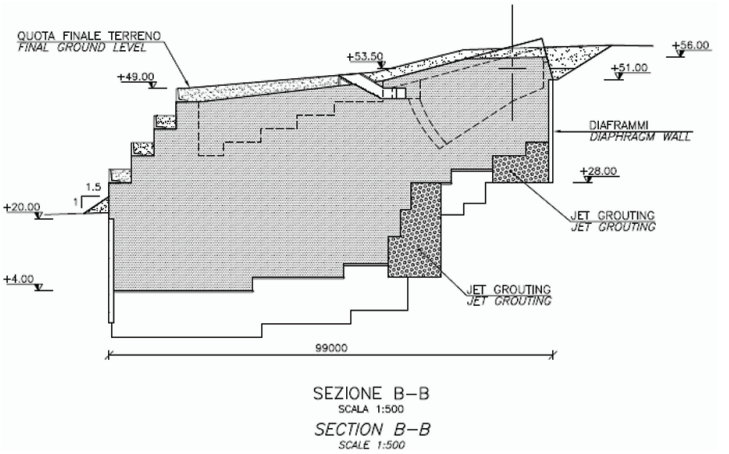

Figure 3.19: Anchorage Block Sicily Side: Section

Chapter 4

Scaled Model

In this chapter, the whole experiment is introduced. The goal of this research was to realize a scaled model of the Messina Strait Bridge, by replacing the existing old model of a cable stayed bridge already built in the laboratory, and to study its dynamic behavior when subjected to ground motion. The bridge was scaled in geometry using a scale factor of 1/265, according to laboratory size, and by means of similitude theory, the similarity in the physical quantities have been found in order to replicate the prototype bridge's behavior. A finite element model of the scaled bridge has been realized on Midas Civil to determine the material to be ordered, used in the construction stage, and to find the natural frequencies. Furthermore, the challenge was to find the deck's cross section and the additional mass to be applied below the deck to have the perfect similarity between the prototype bridge and the scaled one, in terms of static and dynamic match.

4.1 Geometrical Scaling

First of all, was important to determine the scale factor to apply to the Messina Strait Bridge. Understanding its value was essential to determine also all the physical quantities. A primary ispection of the lab was conducted and the old existing bridge dimension was analyzed and as results, the maximum available length that the new bridge could take was of about 13.8 meters (45.2 ft). In the following picture, the old bridge 4.1 and the existing end support 4.2 are shown:

Figure 4.1: Cable-Stayed Bridge: Existing Model

Figure 4.2: Existing End Supports

Knowing the geometrical dimensions of the prototype bridge, was possibile to determine the scale factor to be applied for the scaled model. The prototype bridge has a main

span of 3300 m and both sidespans of 183 m each, with a tower's height of 399 m and equipped with 220 suspenders, as shown in figure 4.3:

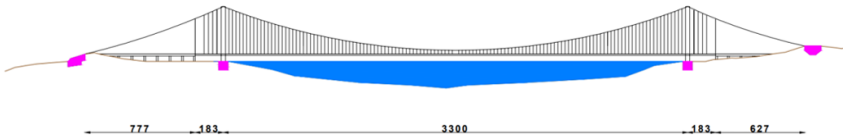

Figure 4.3: Geometrical Review Messina Strait Bridge

From image 4.3 is possible to notice that the total length, assumed as the distance between the two anchor blocks, is about 5070 m. By considering this value the obtained scale factor would have been very small incresing the possibility to have errors during the analysis. For this reason has been chosen to anchor the scaled bridge at a different height allowing to have a bigger scale factor and a more accurate reproduction of the prototype bridge. The scale factor is:

Scale Factor
1/265

Table 4.1: Scaling Factor of the Messina Strait Bridge

That can be applied to all the structural elements composing the bridge, obtaining:

	Prototype Bridge	Scaled Model
Main Span	3300 m	12.5 m
Sidespans	183 m	0.69 m
Towers	399 m	1.51 m

Table 4.2: Scaled Geometrical Dimensions

As regards the cables, has been shown in the previous chapter 3, like in figure 3.15 and 3.16, that both main cables and suspenders are double-type, for this reason, as semplification, both of them are assumed to be a single type by calculating a single equivalent area, because by applying the scale factor wasn't possible to physical represent the double type cables.

4.1.1 Main Cables

In this section, the attention is focused on main cables. By analyzing in detail the official documents of the Messina Strait Bridge has been found that main cables have three different diameters depending on their location along the span, in particular diameters are different between left side span, right side span and main span. They are also double type, and in the next table 4.3 the area of a single cable has been reported:

Location	A [m^2]	*Diameter* [m (ft)]
Left span	1.050	1.156 (3.79)
Main span	1.015	1.137 (3.73)
Right span	1.038	1.150 (3.77)

Table 4.3: Main Cables

In the scaled model, as semplification, the double type cable was substituted with a single one having the equivalent cross sectional area given by the sum of the two of them. Further semplification has been made related to the cable's diameter because a single diameter has been used, obtained as the average value between the three, as representative main cable in the scaled model. In the following table 4.4, details about the diameters and the lenghts of the cables for both prototype and scaled bridge have been reported, noticing that about the length, an additional value of 6 meters has been considered for safety and practical reason.

Prototype	Average single cable area *[m^2]*	1.034
	Average Diameter *[m] (ft)*	1.148 (3.77)
	Area double cable *[m^2]*	2.069
	Equivalent Diameter *[m] (ft)*	1.623 (5.33)
	Length *[m] (ft)*	3800 (12467.8)
Scaled Model	Diameter *[mm] (inch)*	6.12 (0.24)
	Length *[m] (ft)*	14.34 (47.05)

Table 4.4: Main Cable Equivalent Dimensions

The values reported in table 4.4 are related to one half of the bridge and the ordered material is found by doubling all the quantities.

4.1.2 Suspenders

In this section, suspenders are analyzed in more detail. In total 110 suspenders are present per each side and 5 of them are in the side span. The distance between suspenders is 30 m in the prototype bridge and 11 cm in scaled model. Also in this case, as mentioned before, suspenders are double type cable and they have three different diameters depending on the location along the bridge's span. The double type suspender has been simplified with a single one having the equivalent area, but three different diameters are used in the scaled model. In figure 4.4, suspenders pattern is illustrated:

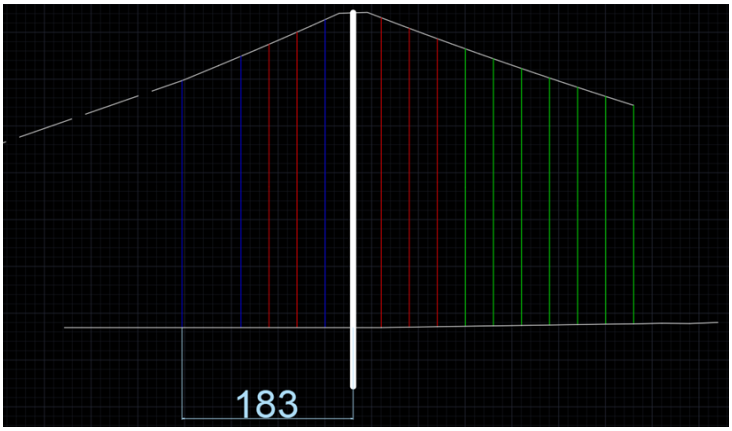

Figure 4.4: Suspenders Configuration

Furthermore, in the next table 4.5, cable's characteristics and properties are reported:

	REAL MODEL				**SCALED MODEL**			
Hanger	A [m^2]	d [m]	A (in^2)	d (in)	A [mm^2]	d [mm]	A (in^2)	d (in)
1,2,5 (blue)	0.038	0.22	0.41	8.66	0.54	0.83	0.00086	0.033
3,4,6,7,8 (red)	0.019	0.16	0.20	6.30	0.28	0.60	0.00045	0.024
9,10,.. (green)	0.014	0.13	0.15	5.12	0.19	0.49	0.00028	0.019

Table 4.5: Suspenders Diameter Configuration

By considering as reference system, the one having the origin located at the center deck level, the following tables 4.6 and 4.7 illustrate coordinates of each suspender with their geometrical characteristics, for only one half of the bridge:

Table 4.6: Suspenders geometric values – 1

REAL MODEL				SCALED MODEL		
Number	**Coordinates [m]**	**Length [m] (ft)**	**Diameter [m] (in)**	**Length [m] (ft)**	**Diameter [mm]**	**Diameter [in]**
1	-1833	264 (866.18)	0.22 (8.66)	0.996 (3.27)	0.033	1.30
2	-1770	290 (951.49)	0.22 (8.66)	1.095 (3.59)	0.033	1.30
3	-1740	303 (994.14)	0.16 (6.30)	1.137 (3.75)	0.024	0.94
4	-1710	316 (1036.80)	0.16 (6.30)	1.178 (3.93)	0.024	0.94
5	-1680	329 (1079.45)	0.22 (8.66)	1.221 (4.07)	0.033	1.30
6	-1620	331 (1086.01)	0.16 (6.30)	1.228 (4.03)	0.024	0.94
7	-1590	320 (1049.92)	0.16 (6.30)	1.198 (3.96)	0.024	0.94
8	-1560	308 (1010.55)	0.16 (6.30)	1.164 (3.81)	0.024	0.94
9	-1530	296 (971.18)	0.13 (5.12)	1.119 (3.67)	0.019	0.78
10	-1500	285 (935.09)	0.13 (5.12)	1.076 (3.53)	0.019	0.78
11	-1470	274 (898.99)	0.13 (5.12)	1.033 (3.39)	0.019	0.78
12	-1440	264 (866.18)	0.13 (5.12)	0.996 (3.27)	0.019	0.78
13	-1410	253 (830.30)	0.13 (5.12)	0.958 (3.13)	0.019	0.78
14	-1380	243 (797.28)	0.13 (5.12)	0.921 (3.01)	0.019	0.78
15	-1350	233 (764.47)	0.13 (5.12)	0.885 (2.89)	0.019	0.78
16	-1320	224 (734.94)	0.13 (5.12)	0.848 (2.77)	0.019	0.78
17	-1290	215 (705.42)	0.13 (5.12)	0.811 (2.66)	0.019	0.78
18	-1260	205 (672.15)	0.13 (5.12)	0.773 (2.54)	0.019	0.78
19	-1230	196 (643.08)	0.13 (5.12)	0.736 (2.43)	0.019	0.78
20	-1200	187 (613.55)	0.13 (5.12)	0.699 (2.29)	0.019	0.78
21	-1170	178 (584.02)	0.13 (5.12)	0.662 (2.20)	0.019	0.78
22	-1140	170 (557.74)	0.13 (5.12)	0.637 (2.11)	0.019	0.78
23	-1110	162 (531.52)	0.13 (5.12)	0.610 (2.01)	0.019	0.78
24	-1080	153 (501.99)	0.13 (5.12)	0.577 (1.89)	0.019	0.78
25	-1050	146 (479.03)	0.13 (5.12)	0.550 (1.81)	0.019	0.78
26	-1020	138 (452.78)	0.13 (5.12)	0.518 (1.70)	0.019	0.78
27	-990	131 (429.81)	0.13 (5.12)	0.496 (1.62)	0.019	0.78
28	-960	124 (406.84)	0.13 (5.12)	0.471 (1.54)	0.019	0.78
29	-930	117 (383.88)	0.13 (5.12)	0.446 (1.45)	0.019	0.78
30	-900	110 (360.91)	0.13 (5.12)	0.420 (1.38)	0.019	0.78

Table 4.7: Suspenders geometric values – 2

REAL MODEL				SCALED MODEL		
Number	**Coordinates [m]**	**Length [m] (ft)**	**Diameter [m] (in)**	**Length [m] (ft)**	**Diameter [mm]**	**Diameter [in]**
31	-870	103 (337.94)	0.13 (5.12)	0.389 (1.28)	0.019	(0.78)
32	-840	97 (318.26)	0.13 (5.12)	0.366 (1.20)	0.019	(0.78)
33	-810	91 (298.57)	0.13 (5.12)	0.343 (1.13)	0.019	(0.78)
34	-780	85 (278.89)	0.13 (5.12)	0.320 (1.05)	0.019	(0.78)
35	-750	79 (259.20)	0.13 (5.12)	0.298 (0.98)	0.019	(0.78)
36	-720	74 (242.79)	0.13 (5.12)	0.281 (0.92)	0.019	(0.78)
37	-690	68 (223.11)	0.13 (5.12)	0.258 (0.85)	0.019	(0.78)
38	-660	64 (209.98)	0.13 (5.12)	0.244 (0.80)	0.019	(0.78)
39	-630	60 (196.86)	0.13 (5.12)	0.226 (0.74)	0.019	(0.78)
40	-600	56 (183.74)	0.13 (5.12)	0.212 (0.70)	0.019	(0.78)
41	-570	52 (170.61)	0.13 (5.12)	0.196 (0.64)	0.019	(0.78)
42	-540	49 (160.77)	0.13 (5.12)	0.185 (0.61)	0.019	(0.78)
43	-510	45 (147.65)	0.13 (5.12)	0.170 (0.56)	0.019	(0.78)
44	-480	41 (134.52)	0.13 (5.12)	0.155 (0.51)	0.019	(0.78)
45	-450	37 (121.40)	0.13 (5.12)	0.140 (0.46)	0.019	(0.78)
46	-420	34 (111.55)	0.13 (5.12)	0.128 (0.42)	0.019	(0.78)
47	-390	30 (98.43)	0.13 (5.12)	0.113 (0.37)	0.019	(0.78)
48	-360	27 (88.59)	0.13 (5.12)	0.102 (0.34)	0.019	(0.78)
49	-330	24 (78.74)	0.13 (5.12)	0.091 (0.30)	0.019	(0.78)
50	-300	21 (68.90)	0.13 (5.12)	0.079 (0.26)	0.019	(0.78)
51	-270	19 (62.34)	0.13 (5.12)	0.072 (0.24)	0.019	(0.78)
52	-240	17 (55.78)	0.13 (5.12)	0.064 (0.21)	0.019	(0.78)
53	-210	15 (49.22)	0.13 (5.12)	0.057 (0.19)	0.019	(0.78)
54	-180	13 (42.65)	0.13 (5.12)	0.049 (0.16)	0.019	(0.78)
55	-150	11 (36.09)	0.13 (5.12)	0.042 (0.13)	0.019	(0.78)
56	-120	10 (32.81)	0.13 (5.12)	0.038 (0.12)	0.019	(0.78)
57	-90	9 (29.53)	0.13 (5.12)	0.034 (0.11)	0.019	(0.78)
58	-60	8 (26.25)	0.13 (5.12)	0.030 (0.10)	0.019	(0.78)
59	-30	7 (22.97)	0.13 (5.12)	0.026 (0.09)	0.019	(0.78)
60	0	7 (22.97)	0.13 (5.12)	0.026 (0.09)	0.019	(0.78)

The total amount of wire to be ordered is obtained by multiplying by four, the sum of the lengths reported in the previous tables. Results are shown below:

To be ordered

Steel wire cable [mm] (ft)	*Length [m] (ft)*
Diameter [0.838] (0.033)	[13.443] (44.1)
Diameter [0.610] (0.024)	[23.835] (78.2)
Diameter [0.483] (0.019)	[83.115] (272.7)

Table 4.8: Material to be ordered for suspenders

4.2 CAD

Based on the previous calculation, the CAD model has been realized and in this subsection all the technical drawings will be reported

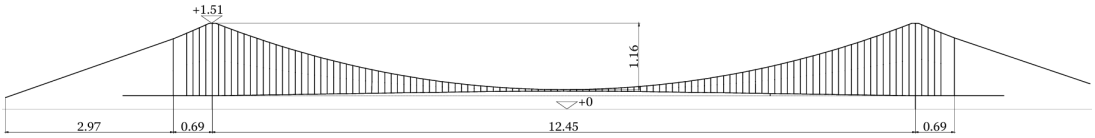

Figure 4.5: Scaled Bridge CAD Model

In figure 4.5 the whole scaled bridge is reported. And in figure 4.6 the tower's technical drawing is shown.

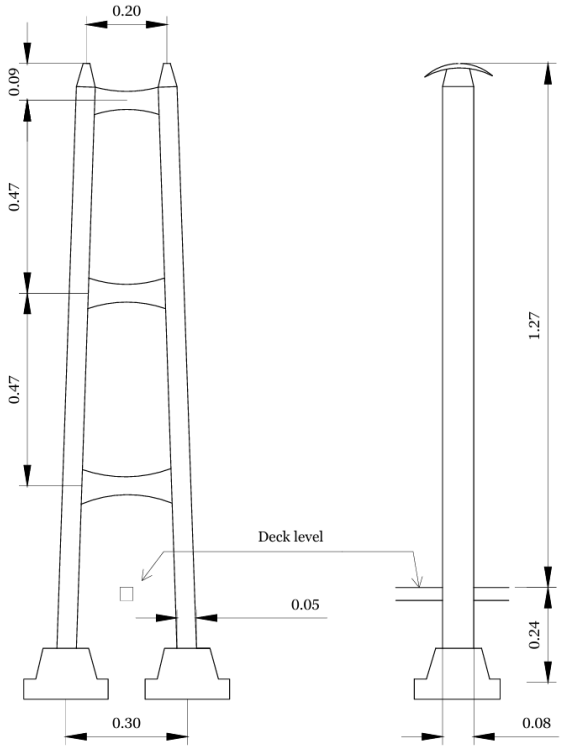

Figure 4.6: Scaled Towers CAD Model

As regards the selection of the deck's cross section and tower's cross section, calculation are based on similitude theory [13] and numerical analysis realized on Midas Civil which will be illustrated in following sections.

4.3 Similitude Theory

As previous mentioned, the scaled model was constructed at a 1/265 scale, respecting the maximum available size of the laboratory. The main objective of this research is to replicate as close as possible the dynamic response of the Messina Bridge. To accomplish this result, similitude theory has been used [13]. This theory allow to replicate and predict the behavior of a real structure by doing considerations on dimensional analysis. Dimensional analysis is very important while studying physical phenomena and allows to organise variables into simplified dimensionless groups called Pi terms by reducing the number of indipendent parameters [13]. Similitude theory is based on Buckingham's Pi Theorem and according to this theorem, any equation containing physical variable can be expressed as an equivalent expression with dimensionless parameters. In the context of structural modelling, this implies that the mathematical formulation describing a physical quantity such as

$$F(X_1, X_2, \ldots, X_n) = 0 \tag{4.1}$$

can be equivalently expressed in terms of non-dimensional terms, in the form of:

$$G(\pi_1, \pi_2, \ldots, \pi_n) = 0 \tag{4.2}$$

The pi terms are identified like a combination of physical quantities that are dimensionless such as $X_1, X_2, \ldots, X_n$. These terms are formed by m = n – r independent and non-dimensional expressions, where n is the number of physical quantities and r is the number of fundamental dimensions. In the particular case of structural modelling, applying this theory, three main categories can be identified [13]:

1. *Exact (or fully similar) model*: In this type of category, all the similarity requirements are satisfied. Therefore, when a model satisfies every similarity criteria, it is considered to have a complete similarity with the prototype.

2. *Approximate (or first-order) model*: In this case only the first order similarity is obtained and it is related to have an exact replication of the moment of inertia while neglecting the exact scaling of the cross sectional area. Therefore, models that meet the primary order similarity conditions are involved in this category.

3. *Distorted model*: In this category there is not a match with one or more first order conditions obtained by dimensional analysis.

Even if the main objective is always to get the full similarity, often, for practical reason, such as cost and experimental limitations, this result cannot be obtained. But by neglecting some second order considerations, a sufficient accurate model that could reflect a real behavior could be designed [13]. In general, when a model has complete similarity, the mathematical description that is based on Buckingham's theorem can be presented in the following form:

$$\pi_1 = \phi(\pi_2, \pi_3, \ldots, \pi_n) = 0 \tag{4.3}$$

If relationship (4.3) is written once for the prototype and once for the model, it becomes possible to form a ratio between corresponding quantities. In particular:

$$\frac{\pi_{1p}}{\pi_{1m}} = \frac{\phi(\pi_{2p}, \pi_{3p}, \ldots, \pi_{np})}{\phi(\pi_{2m}, \pi_{3m}, \ldots, \pi_{nm})} \tag{4.4}$$

Where, π_{1m} refers to π_1 in the model and π_{1p} refers to π_1 in the prototype, etc. Complete similarity is defined as the condition in which all dimensionless products have the same values in both the model and the prototype. When this condition is matched, the relationships become:

$$\begin{aligned} \pi_{2m} &= \pi_{2p} \\ \pi_{3m} &= \pi_{3p} \\ &\vdots \\ \pi_{nm} &= \pi_{np} \end{aligned} \tag{4.5}$$

in a way that equation (4.4) can be writtes as:

$$\frac{\pi_{1p}}{\pi_{1m}} = \frac{\phi(\pi_{2p}, \pi_{3p}, \ldots, \pi_{np})}{\phi(\pi_{2m}, \pi_{3m}, \ldots, \pi_{nm})} = 1 \tag{4.6}$$

which leads to:

$$\pi_{nm} = \pi_{np} \tag{4.7}$$

This consideration expresses the fact that if complete similarity is obtained, the behavior observed in the scaled model can be directly associated to the one in the prototype. In this research, the obtained scale factors for the physical quantities are reported in the following table:

Physical Quantity	**Similarity Relation**	**Dimension**	**Scaling Factor**
Length (L)	S_L	L	$\frac{1}{265} = 0.0038$
Elastic Modulus (E)	S_E	FL^{-2}	1
Acceleration (a)	S_a	LT^{-2}	1
Stress (σ)	S_σ	FL^{-2}	1
Force (F)	S_F	F	$\left(\frac{1}{265}\right)^2 = 0.000014$
Strain (ε)	S_ε	$-$	1
Time (t)	S_t	$T = L^{1/2}$	$\left(\frac{1}{265}\right)^{1/2} = 0.0614$

Table 4.9: Physical Quantities Scaling Factors

In particular, given that the same material of the prototype bridge has been used to build the scaled model, the scaling factor for elastic modulus is set as one. Then, the bridge has been designed to have the same stresses of the prototype one and for this reason also the stress scale factor is set as one. Furthermore, both bridges are assumed to be subjected to the same gravity fields, therefore the acceleration scale factor is also set as unit value. Particular attention should be given to the scale factor for the time, because it plays a very important role for this research as it is used to scale natural periods of the prototype, in order to obtain the target one, and also to scale in time the applied input ground motion during numerical and experimental analysis. In terms of static analysis, the force in each suspender P_{prot} is obtained from the deck linear weight which is 23 t/m, equivalent to 230 KN/m. Considering the space of 30 meters between the suspenders, the load in each of them is about:

$$P_{\text{prot}} = 230\,\text{kN/m} \times 30\,\text{m} = 6900\,\text{kN} \tag{4.8}$$

Instead, the natural period of the prototype bridge are the following ones:

Periods [s]	
Mode nº	**Prototype real scale**
1	33.17
2	18.23
3	15.44
4	12.59
5	12.43
6	12.43
7	12.42
8	12.38
9	11.05
10	10.25

Table 4.10: Vibration Modes and Corresponding Natural Periods of Prototype Bridge

Specifically, for the hangers, the relationship between the stress values in the prototype and the scaled model can be described as follows:

$$\frac{P_{prot}}{A_{prot}} = \frac{P_{model}}{A_{model}} \tag{4.9}$$

And developing the equation, using the scaling factor for the force S_F, the force of each hanger is:

$$P_{model} = P_{prot} \times \frac{1}{265^2} \tag{4.10}$$

From analysis conducted previously on the prototype bridge, the stress in each hanger is known and the equivalent weight to be attached at each hanger to have similarity in the stresses is:

$$P_{\text{model}} = \frac{6900}{265^2} = 0.098\,\text{kN} \approx 10\,\text{kg} \tag{4.11}$$

At this point, due to laboratory and experimental limitation it would not have been possible to apply a load of 10 kg per each hanger because of the size of it. Furthermore, given the flexibility and slenderness of the deck, the application of this load could have caused excessive deflection increasing the risk of damage in structural components of the scaled model. For this reason, the choise of using 1 kg per hanger has been made, neglecting the match in the static profile and to try to reach as close as possible the dynamic similarity. In the next table, results of stresses in the cables are reported:

Element	**Prototype [MPa]**	**10 kg Scaled Model [MPa]**	**Actual Scaled Model [MPa]**
Main cable	580	530	113
Hangers	345	335	87.5

Table 4.11: Cable's Stresses

Has been noticed that by putting a weight of 10 Kg per hanger, the stresses in the cables are very close to the stresses in the prototype bridge, showing an high accuracy in the similarity laws. As regards dynamic similarity, the scaled natural period are obtained from the following relationship:

$$T_{mod} = T_{prot} \cdot S_t \tag{4.12}$$

and in the particular case of the first one, for example, the following value is obtained:

$$T_{mod} = T_{prot} \cdot S_t = 33.17 \cdot \left(\frac{1}{265}\right)^{1/2} = 2.045 \; sec \tag{4.13}$$

By repeating the same calculation for all modeshapes, the target natural period for the first 10 modeshapes are shown in the following table:

Periods [s]		
Mode nº	**Prototype**	**target**
1	33.17	2.045
2	18.23	1.119
3	15.44	0.948
4	12.59	0.773
5	12.43	0.764
6	12.43	0.764
7	12.42	0.763
8	12.38	0.760
9	11.05	0.679
10	10.25	0.630

Table 4.12: Vibration Modes and Natural Periods of Prototype and Scaled Bridge

Some important observations related to the natural period are carried out, in particular, given that in this research the focus is about ground motion application, the most relevant modes are the transversal ones and therefore the cross section has been designed based on this assumption. To find the structural elements cross section to have similarity in the natural periods, a FE model on Midas Civil has been created and different analysis with different cross section are carried out. Further information are provided in the next section, related to the FE model. In particular, has been noticed how a good compromises is obtained by using, for the deck, a HSS square cross section ($1\frac{1}{4} \times 1\frac{1}{4} \times \frac{1}{8}$ in) with a plate of 1.5 kg and additional 1 kg weight to reach the total amount of 3.5 kg. Unfortunately, as mentioned and explained before, the perfect similarity could not be reached due to laboratory limitations. As regards the suspension system, perfect geometric similarity is obtained because main cables have a wire diameter of 6.35 mm and suspenders have a diameter of 0.5 mm, 0.6 mm and 0.8 mm.

4.4 Finite Element Model

A finite element model of the scaled bridge has been realized on Midas Civil 4.7. The main purpose was to better understand which cross section should be used to respect the similarity in dynamic analysis. In particular, deck and towers are modelled as beam elements and suspension system is modelled as truss elements. A total of 621 nodes and 624 elements are present.

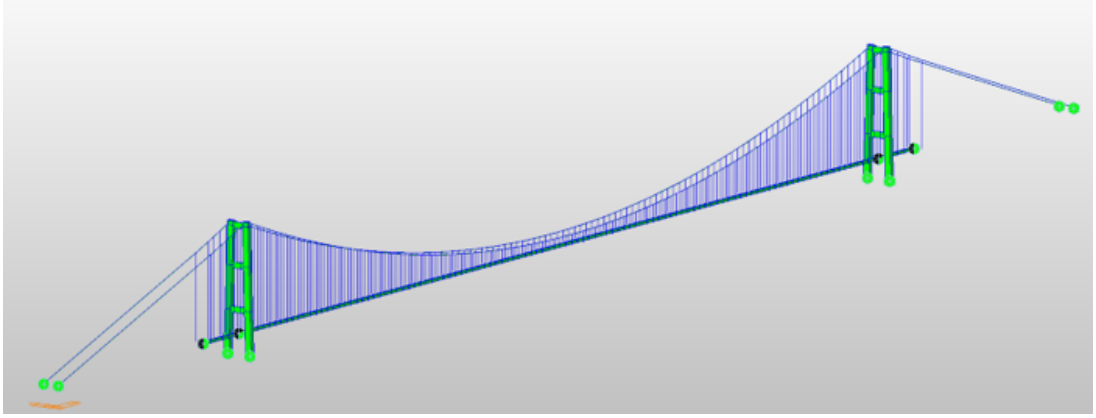

Figure 4.7: Scaled Bridge FE Model

Is important to cite the semplification used during this phase. In particular, the deck element has been modelled as straight, while the one in the prototype has a slight upward inclination in the center span. Furthermore, both double type main cables and suspenders are modelled as single cable with an equivalent area because after scaling, the spacing between the two wires would have been negligible.

4.4.1 Geometry

The bridge model was realized using the suspension bridge wizard tool present on Midas Civil. This tool allows to design a simplified model by providing the coordinates of towers, deck and sag and also providing the spacing between suspenders.

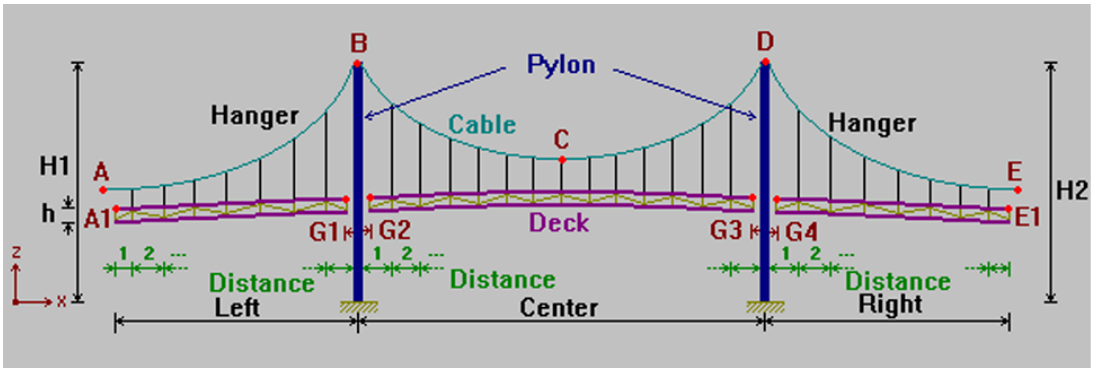

Figure 4.8: Coordinates FE model

An important consideration should be done about sag point C, because the software provides convergency only at a height of 0.36 m, while it should lie at a height of 0.27m. The reason behind this, could be assigned to the fact that the prototype bridge has an

upward curvature while in the scaled model a semplified straight deck has been used. Coordinates are illustrated in the next table:

Point	x [m]	y [m]	z [m]
A	0.00	0.00	0.24
A1	2.86	0.00	0.24
B	3.66	0.00	1.51
C	9.89	0.00	0.36

Table 4.13: Coordinates of key points in the model

As regard the towers, the height has been set as 1.51 m, in accordance with the geometric similarity obtained in similitude theory. Same considerations are carried out about suspenders, by setting a distance between them of 0.115 m, in order to have the correct number in the model. The deck cross section is HSS ($1\frac{1}{4} \times 1\frac{1}{4} \times \frac{1}{8}$ in) and the tower's cross section is a HSS $3 \times 2 \times 8/12$ inch. Furthermore, in order to have a good representation of the model that could respect the geometric similarity, the towers have been modelled with an inward inclination, by setting a distance at the base of 30 cm and a distance at the top of 20 cm. Furthermore, in each tower are present three cross beams that connect the two legs, replicating the real geometry of the prototype bridge.

4.4.2 Boundary Conditions

The boundary condition applied to the FE model are chosen referring to the reference model, in order to have similarity in the modeshapes. For this reason, fixed constraints are used for anchorage blocks and base of the tower, then rollers are used at the connection between the deck and the towers and hinges are used as end supports. Furthermore, to represent differrent soil conditions, the addition of linear springs are placed at the base of the tower to simulate the spring box system designed for the experimental setup.

Rigid	**Support**	**Dx**	**Dy**	**Dz**	**Rx**	**Ry**	**Rz**
	End Support	1	1	1	0	0	0
	Tower Support	0	1	1	0	0	0
	End Cable Support	1	1	1	1	1	1
Elastic	**Support**	**KDx**	**KDy**	**KDz**	**KRx**	**KRy**	**KRz**
	West Tower	1	K	1	1	1	1
	East Tower	1	K	1	1	1	1

Table 4.14: Rigid and Elastic Boundary Conditions

As regard the elastic spring supports, three scenarios have been selected:

- *High stiffness*: K = 200 N/mm
- *Medium stiffness*: K = 20 N/mm
- *Soft stiffness*: K = 4 N/mm

4.4.3 Configurations

Modal analysis has been performed with different deck cross section configuration in order to select the geometry that could provide the best similarity in terms of dynamic analysis and natural periods. Different cross sections have been investigated, without any additonal masses and the results are reported in the following table 4.15:

Section Type	**First Natural Period [s]**
HSS $1\frac{1}{4} \times 1\frac{1}{4}$	0.77
HSS 2×1	0.53
HSS 1×2	0.69
HSS 2×2	0.48
HSS 3×2	0.45
HSS $\frac{1}{2} \times \frac{1}{2}$	0.93

Table 4.15: Natural periods for different HSS sections

All the previous calculation are performed without additional masses and even if the highest natural period is the one obtained with the cross section HSS 1/2 × 1/2, the chosen one is the HSS 1 1/4 × 1 1/4 because the previous one was very slender and we could have had deflection and yielding problem during ground motion application, even if has been studied that in its final configuration composed by an additional weight of 3.5 kg (1.5 kg of plate and two 1 kg additional masses) the period of 2.076 s could have be reached obtaining a result close to the target period of 2.045 s. The last step, before performing the analysis was the definition of the external load. To simulate the plate weight and additional masses for a total weight of 3.5 kg, nodal load of 17.5 N at each hanger has been applied, because is supposed that at each hanger location the weight is 1.75 kg. Nodal loads are then converted into self weight and all the different analysis could be carried out.

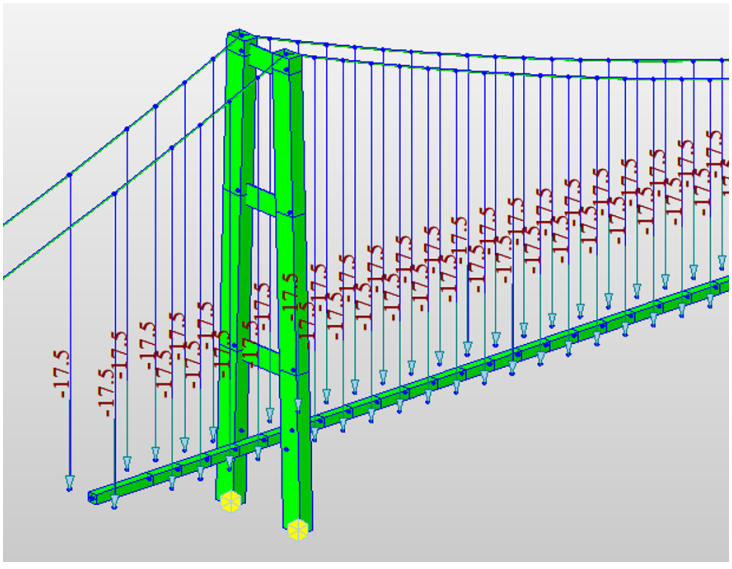

Figure 4.9: Load on each Hanger in FE model

4.4.4 Eigenvalue Analysis

The eigenvalue analysis was used to identify the dynamic properties of the bridge, in particular to find the modeshapes and the natural periods. In particular, Midas provides the Lanczos eigenvalue analysis with which the first ten natural periods have been investigated and reported in the following table:

Mode No.	Period [sec]	Mode Shape
1	1.652	Horiz.
2	0.826	Horiz.
3	0.661	Vert.
4	0.475	Horiz.
5	0.437	Vert.
6	0.299	Horiz.
7	0.259	Vert.
8	0.257	Vert.
9	0.203	Horiz.
10	0.188	Vert.

Table 4.16: Natural Periods of FE Scaled Model

From the results, can be noticed how the third and the fifth natural period are vertical and therefore they have not been taken into account because they are not the primary interest on this research. The focus was assigned to the horizontal modeshapes, in particular the first, the second and the fourth one because they play a more important role for the goals of this study.

Figure 4.10: 1st Modeshape: Prototype - Numerical

Figure 4.11: 2nd Modeshape: Prototype - Numerical

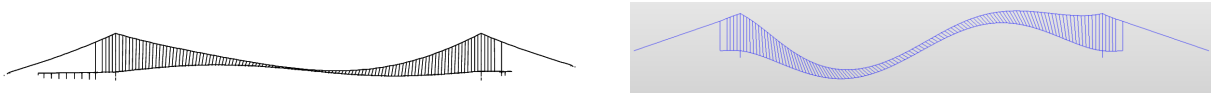

Figure 4.12: 3rd Modeshape: Prototype - Numerical

Figure 4.13: 4th Modeshape: Prototype - Numerical

Figure 4.14: 5th Modeshape: Prototype - Numerical

A comparison between theoretical and numerical model, for the interested mode, is reported in the following table:

Mode	**Prototype** [s]	**Theoretical**	**Numerical**	**Error** [%]
1	33.17	2.045	1.652	19.3
2	18.23	1.119	0.826	26.7
4	12.59	0.773	0.475	38.5

Table 4.17: Theoretical and Numerical Periods Comparison

The obtained error is due to the small mass applied to the system, only 1 kg per hanger, instead of the calculated 10 kg per hanger obtained by mean of similitude theory.

4.5 Construction Stage

In this section, the ordered material and the costruction phase for assembling the bridge have been illustrated. The square HSS cross section ordered for the deck is the following one. The material has been ordered as two deck tube that are then welded in the laboratory at the desired length.

Figure 4.15: Deck Tube

The deck was equipped with steel plates welded below it and 1 kg additional masses placed at each hanger's location. Steel plates are used as support to place addition masses and also to provide a surface to screw suspenders. For this reason in steel plates holes, with a distance of 20 cm, have been drilled to allow hangers connection.

Figure 4.16: Ordered Plate

Figure 4.17: Plate - Drilling Stage

Figure 4.18: Completed Plate

The masses are welded, over the deck, in the following configuration:

Figure 4.19: Additional Steel Cube Weight

The connection between suspender and deck has been obtained by cutting steel bars, provided with nuts, with a length of 3.80 cm. The ordered material was composed by five steel bars of 1.8 meters long each, and a total of 500 nuts.

Figure 4.20: Bars used to create Suspender's Connection

The cutting, in order to obtain the single suspender's anchorage, has been done by using a band saw:

Figure 4.21: Band Saw

Resulting in the following pieces:

Figure 4.22: Suspender Supports

Using this method, over 240 anchoring components were created. In the last step, a transverse hole was drilled in each piece in a way that the wire could pass through it. To lock the hanger in place, the cable was securely twisted at its end and looped around a metallic ring, as shown in figure 4.23 and figure 4.24. The nuts are used to set and adjust the suspender's tension and fine-tuning process.

Figure 4.23: Drilling Procedure

Figure 4.24: Finished Suspender

The suspenders are finally connected to the main cables by using hollow clamps:

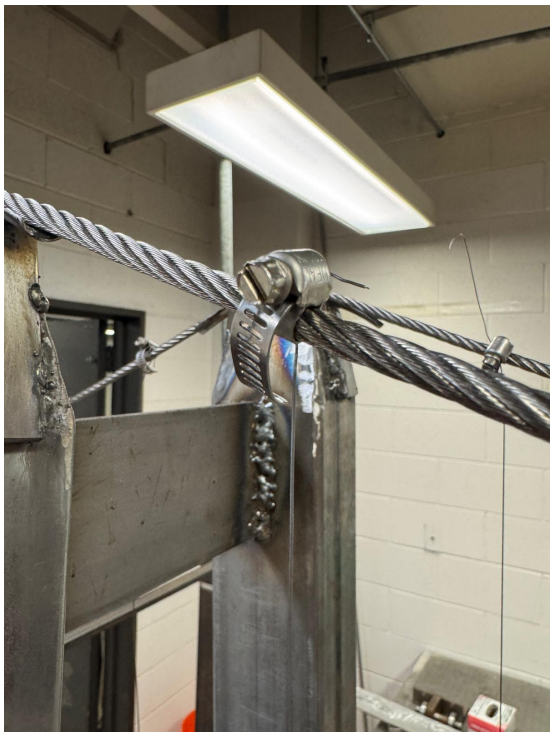

Figure 4.25: Suspender - Main Cable Connection

As regards the tower, HSS 3 x 2 x 1/12 inch profile has been ordered. The raw material, originally ordered, is shown in picture 4.26.

Figure 4.26: Raw Material for Towers

Furthermore, additional steel plates, used as cross beams have been ordered. In particular they have a thickness of 0.4 mm and a width of 75 mm. Each plate was then welded at their location. Result is:

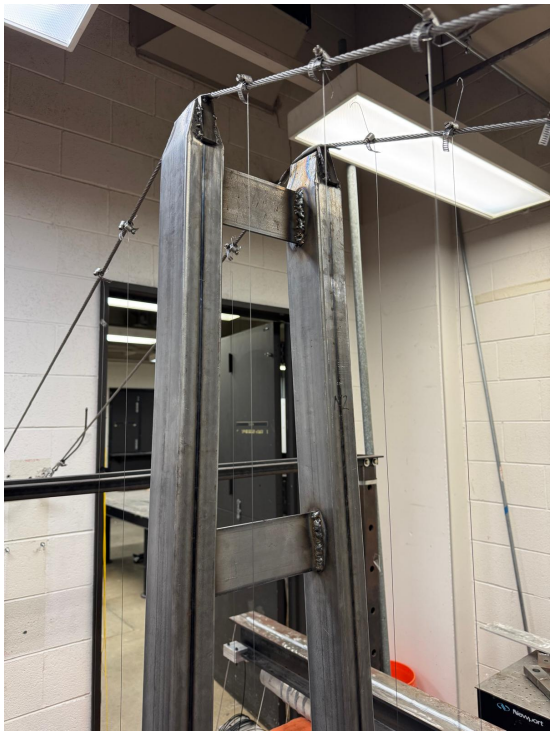

Figure 4.27: Tower's Cross Beams

It is important to note that a saddle was welded at the top of each tower to create a frictionless system.

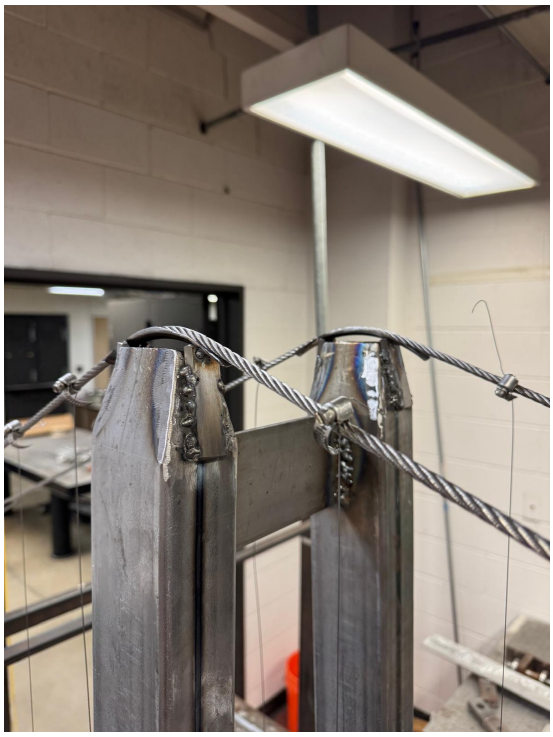

Figure 4.28: Tower's Saddle

The completed configuration of the two towers, is illustrated in figure 4.29. At the base, steel plates used as support for the spring box system are also showed.

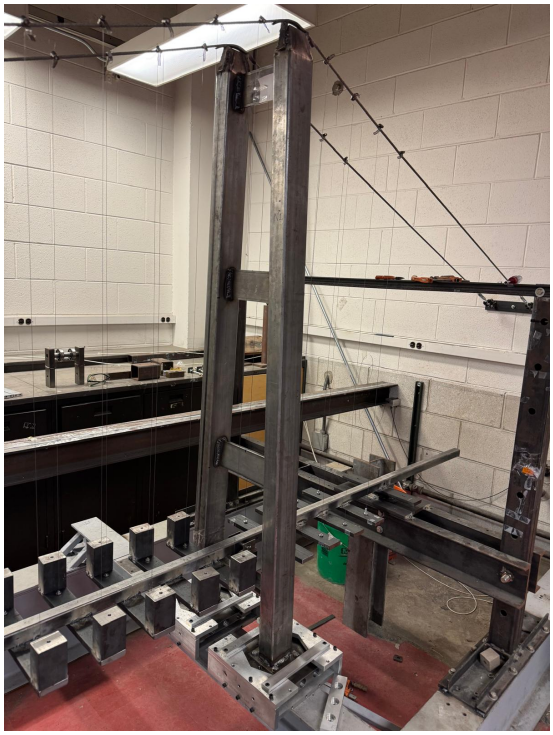

Figure 4.29: Finished Tower

The used anchorages are built by using steel plates bolted to the wall. The system was provided by an adjustable screw used to control the main cable's tension for fine-tuning process.

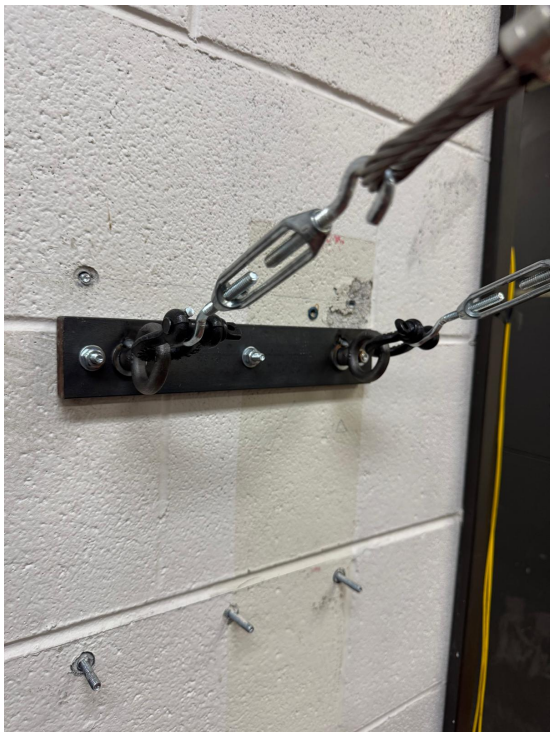

Figure 4.30: Anchorages

As results, the completed bridge is the following one:

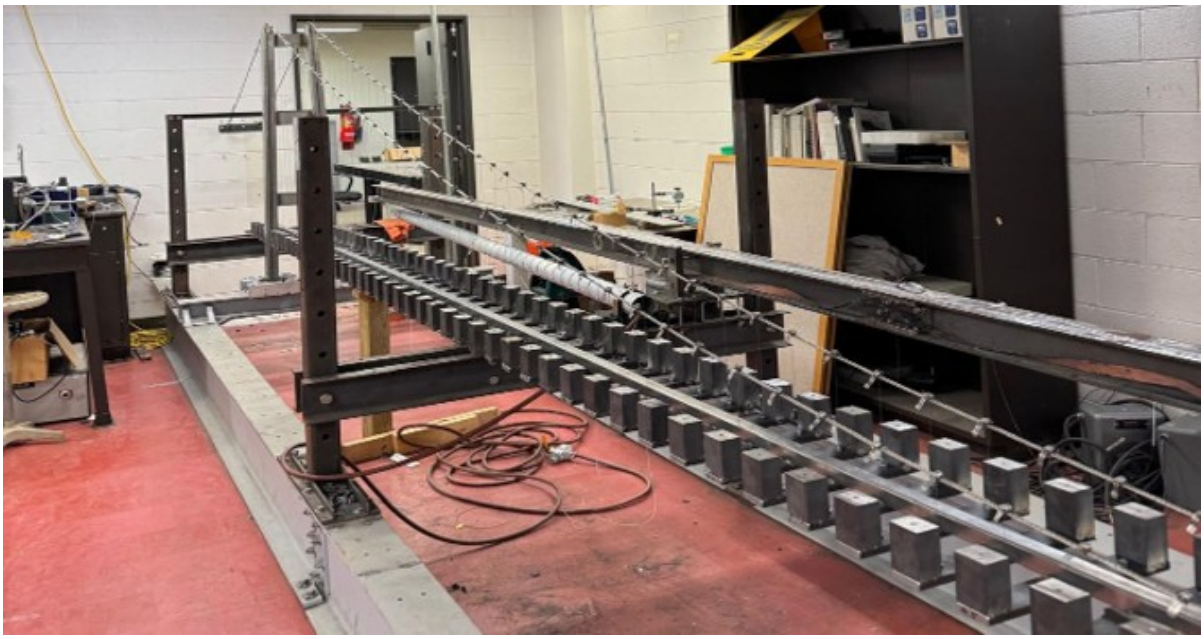

Figure 4.31: Completed Scaled Bridge Model

Chapter 5

Numerical Analysis

This chapter has explored the influence of suspender loss on the structural behavior of the scaled model of the Messina Strait Bridge. Using numerical analysis, member removal analysis by studying DCR [19] has been conducted to evaluate suspension bridge response under sudden suspender failure. In suspension bridge, suspenders play a critical role by transferring loads from the deck to the main cables [19]. Due to their slender geometry and small cross section, suspenders are more susceptible to accidental damage and their vulnerability is increased by their exposure to public access and proximity to high speed traffic [18]. An other very important reason that could lead to suspender failure is its environmental exposure. Suspenders are very slender elements very sensitive to humidity which combined with oxygen could lead to a fast corrosion of steel wire. In addition, wind and vehicle loads can accelerate the damage and the failure in suspenders [16]. Understanding this behavior is essential for assessing the bridge's resilience. To have a better understanding of the structural elements, all the components of the bridge have been labelled. In total the model is composed by 621 nodes and 624 elements and in particular, main cables are numbered from MC01 to MC122 and suspenders are numbered from SUS01 to SUS119. Furthermore, the bridge has been divided in the two planes, and all the components on the second plan have the same name of the ones on the first plan but they are distinguished with an apostrophes, for example MC01' or SUS01'. The labelling is shown in the next figure 5.1.

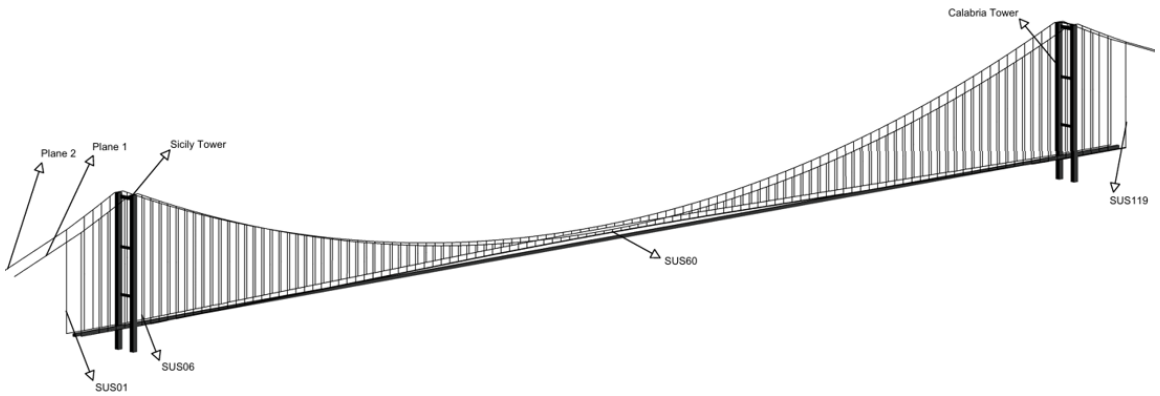

Figure 5.1: Structural Element's label

As first analysis, the behavior of the bridge in undamaged condition and under dead load has been conducted, by setting the self weight as 0.027 KN/m and by considering

the additional masses below the deck that are used to get a dynamic match as close as possible to the theoretical one. In the next table 5.1, the deflection results are reported:

Load Case	**Left span**	**Central span**		**Right span**
	Max	Max	Min	Max
Dead Load	0.011 mm	0.128 mm	-0.263 mm	0.011 mm

Table 5.1: Vertical Deflection - Undamaged

Is important to notice that the upward deflection recorded is related to the adjust in the pretension in the cables. The pre-tensioning is essential to ensure that the bridge assumes its intended design profile and to allow the achieving of the correct equilibrium configuration, as seen also in [19]. From results related to the main cable, has been notice how the tension, under dead load, is in a range between 3027.56 N and 3255.54 N showing that the maximum tension is obtained in elements MC06 (MC06') and MC117 (MC117') that are the one close to the tower and the minimum tension in obtained in elements MC61 (MC61') and MC62 (MC62'), located in the mid-span.

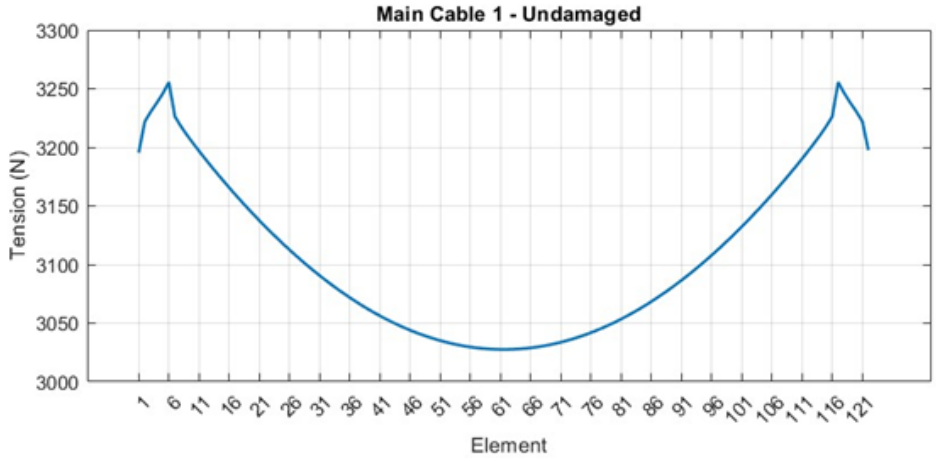

Figure 5.2: Tension Main Cable - Plan 1 - Undamaged

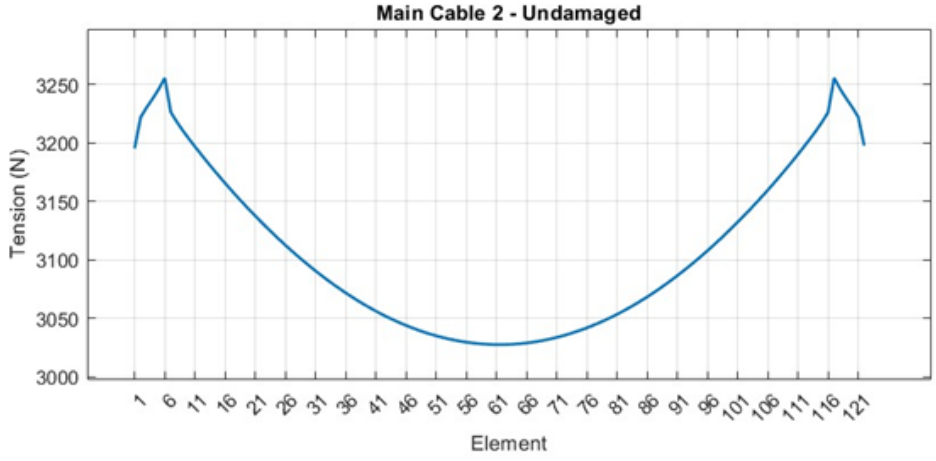

Figure 5.3: Tension Main Cable - Plan 2 - Undamaged

In figure 5.4, the tension profile of suspenders is reported. In particular only suspender that goes from SUS06 to SUS60 are illustrated due to simmetry and has also been noticed that suspenders located in the side spans have a small anomalies in convergence due to the high scale factor used in this project. For this reason only the suspenders in the main span are analyzed and the previous mentioned anomalies does not have an influence on the main span results because the presence of the saddle located at the tower isolates the sidespan from the main span. This lead to a preservation of the validity of the obtained results.

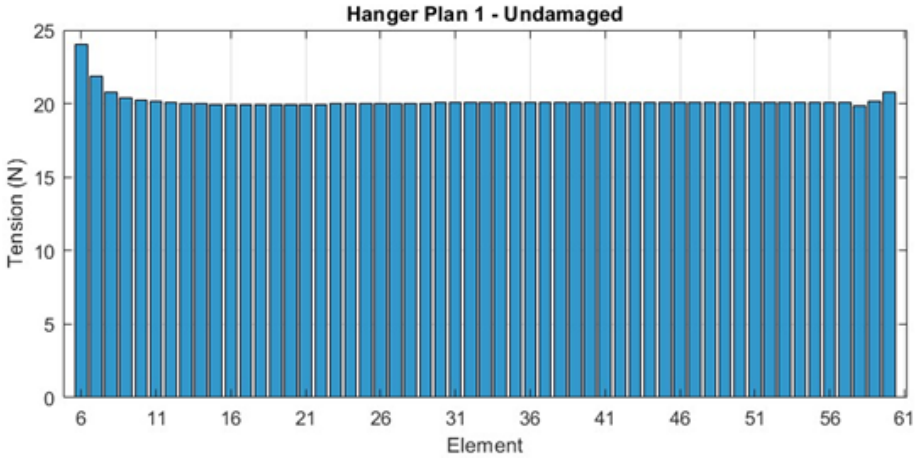

Figure 5.4: Tension Suspender - Undamaged

From the previous figure can be noticed how the suspenders tension is in a range between 19.83 N and 24.03 N. The highest tension of 24.03 N is recorded in the suspender SUS06, the closest one to the tower. On plan 2, results are the same. Member loss analysis is a widely recognized technique employed to evaluate the structural robustness of civil engineering systems. The principle is that a structure can be considered robust against progressive collapse if it retains the ability to redistribute internal forces and create alternative load paths following the sudden loss of a single critical member [19]. Given the simmetry of the structure, only one half of the bridge has been subjected to DCR analysis, in particular only suspenders in the range of SUS06 to SUS60 are studied. During this analysis 55 simulation have been performed in order to identify which cable loss scenario could generate the worst and most critical response that was useful to understand where to place the sensors in the experimental analysis. The worst scenario was obtained by studying the Demand to Capacity ratio (DCR) that is used as a performance indicator that is obtained by comparing the stress S to the capacity C, usually defined as yield strength [19].

$$\text{DCR} = \frac{S}{C}$$

- S is the stress of a suspender after damage
- C is the capacity of the suspender (yield strength)

In this case C is 1170 MPa. When DCR value is higher than unity, indicates that the demand is higher than the capacity and this lead to the collapse of the structural element. By conducting this analysis for all the suspenders, the highest DCR value has been recorded for each scenario and that specific value has been considered as the most critical

one. The maximum value in a scenario analyzed is then used as representative value of the damage induced by that specific suspender loss case. After comparing the DCR values in all the analyzed scenario is possible to identify the worst condition, that is the case in which the suspender loss could lead to a progressive collapse of the other suspenders and potentially compromise the overall stability of the bridge. By removing cables sequentially from suspender SUS06 to SUS60, the DCR value are plotted and results are shown in figure 5.5. From analysis in the undamaged state, DCR values are in a range between 0.063 and 0.090 but when cables are removed, DCR values are in a range between 0.086 to 0.132 showing a remarkable increase in the tension as result of the redistribution of the forces in a new load path.

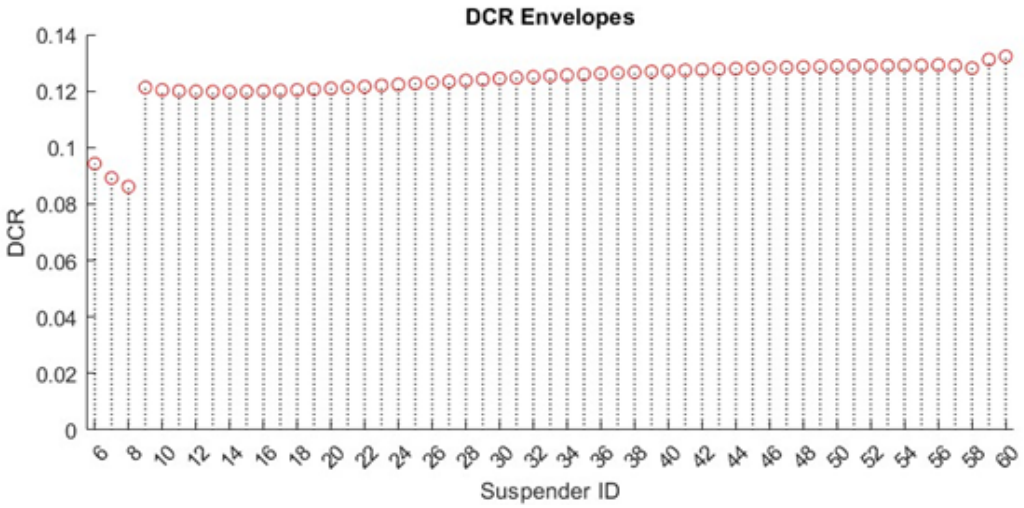

Figure 5.5: DCR Envelopes

From figure 5.5 has been noticed that the highest DCR is obtained in the SUS60 that is obtained when SUS59 is removed. For this reason SUS59 has been identified as the worst scenario and it has been taken into account to represent the dynamic bridge's behavior in damaged condition. From numerical analysis obtained in static conditions, and by focusing the attention to local deflection and changes in suspenders and main cable forces, can be noticed how results reveal how the damage is highly localized and how the impact of the suspender loss is very slight in farther structural elements. The vertical displacement profile after member removal is compared to the one in the intact bridge in the following figure 5.6, showing the localized effect of suspender loss in vertical deflection. By zooming into the effected area, figure 5.7, some differences are noted in proximity of SUS59, showing and increase in deflection of the 5.5% with values that goes from an initial displacement of 0.121 mm to a final one of 0.128 mm.

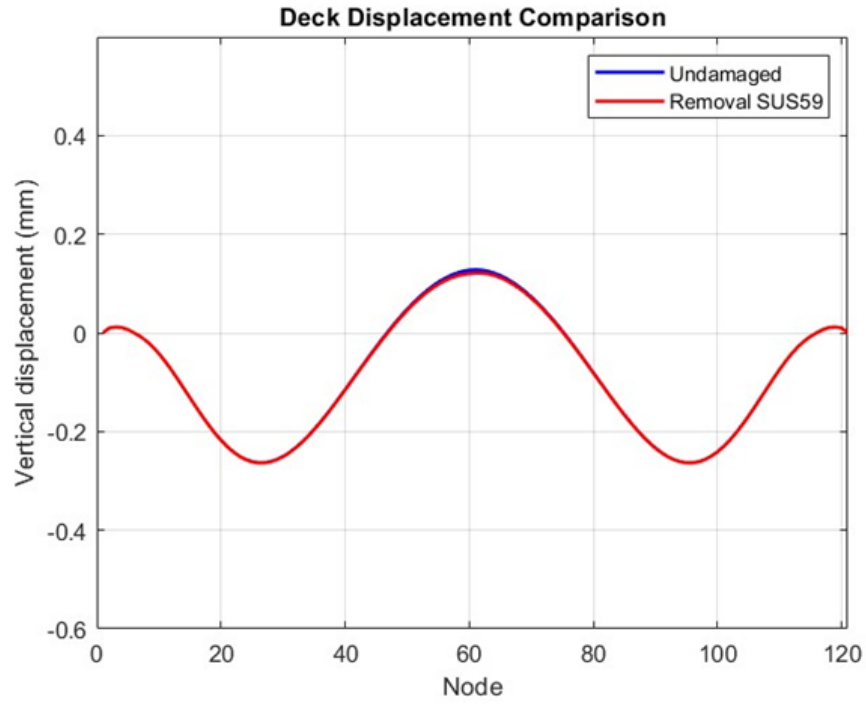

Figure 5.6: Comparison in Deck Displacement

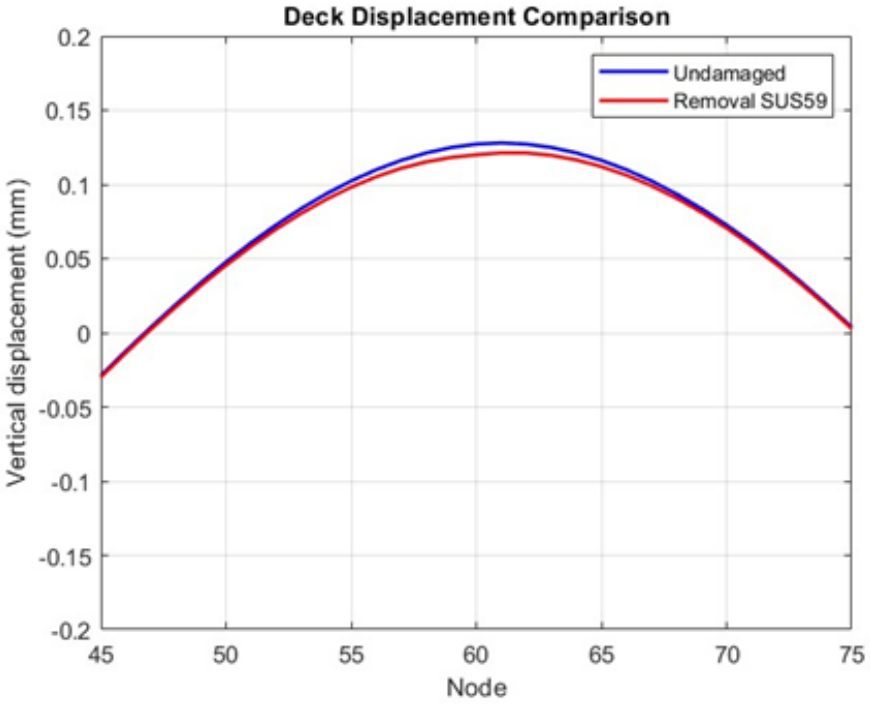

Figure 5.7: Localized Deck Displacement Comparison

As regards the main cables, also in this case a comparison between the tension obtained after SUS59 removal and the undamaged configuration has been investigated and results illustrated in figure 5.8 show how the effect of suspender loss has a minimal and negligible influence on the main cables tension profile.

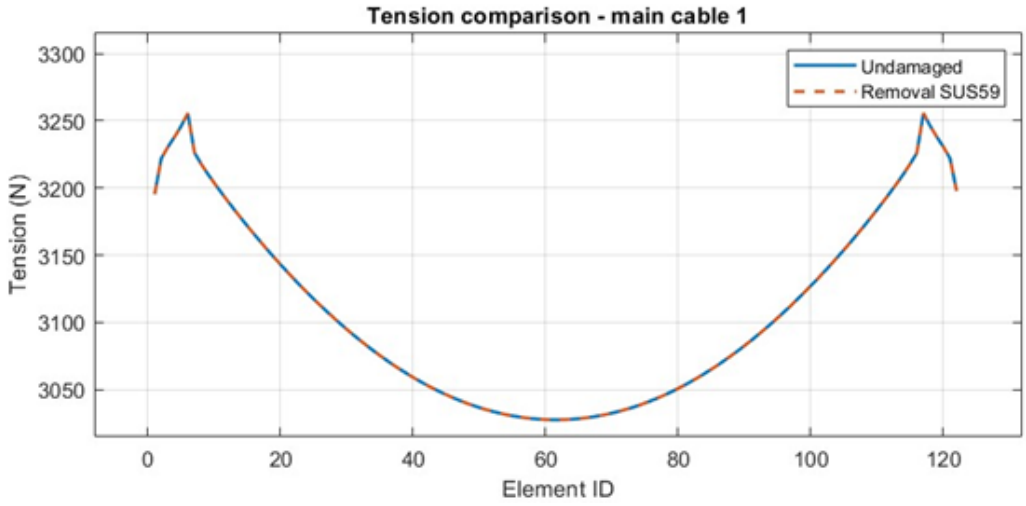

Figure 5.8: Main Cable Comparison Damaged and Undamaged

Instead, more important findings are obtained related to the suspenders tension profile. In particular the localized effect has been investigated more in detail in suspenders ranging from SUS56 to SUS62 and results show the highly localized effect of the suspender removal by recording a remarkable increase in tension in the suspender adjacent to the broken one. The results are illustrated in figures 5.9 and 5.10 for both planes showing that cable loss in one plan has a very slight influence on the bridge's opposite side. The changes in tension recorder in SUS56, SUS57, SUS61, and SUS62, are smaller with respect changes observed in suspender SUS58 and SUS60. All these findings confirm the localized nature of the damage with the conclusion that the effect of a single suspender failure do not propagate across the plane.

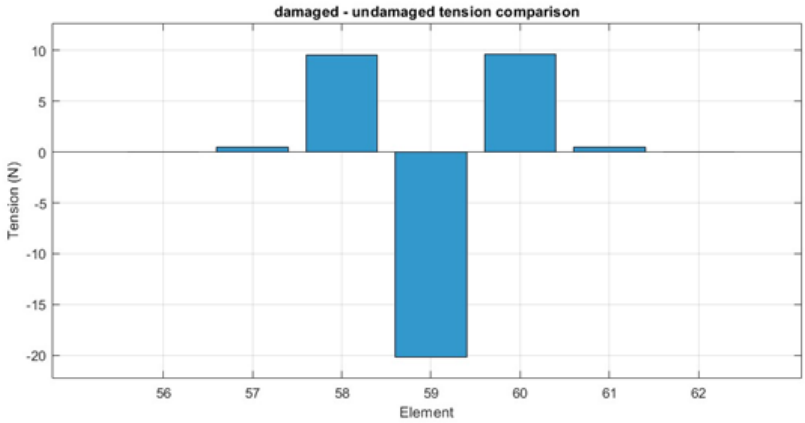

Figure 5.9: Tension After Damage - Plan 1

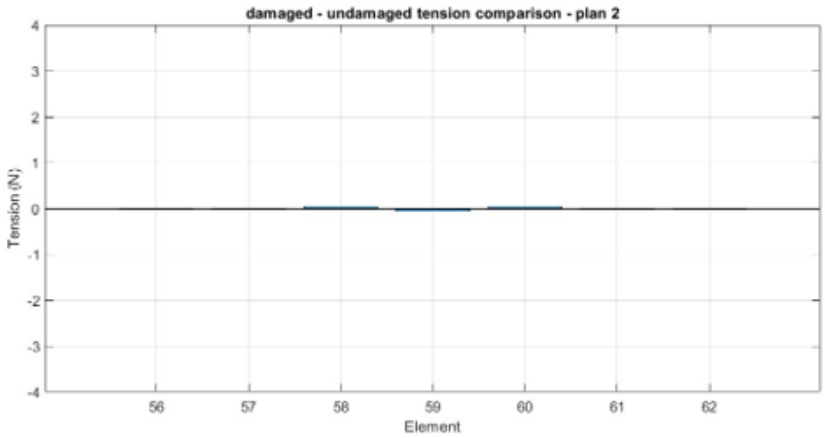

Figure 5.10: Tension After Damage - Plan 2

The conducted analysis was useful to understand where to place the sensor in the experimental model, because one of the goal of this study was to investigate the dynamic behavior of the bridge in damaged configuration. But given that performing this analysis on the numerical model was not possible due to Midas Civil limitation, the study was postponed on the experimental one, which is still waiting to be completed and investigated.

Instead undamaged condition were investigated on numerical model and for this purpose two earthquakes and three soil condition have been selected to investigate the bridge's dynamic behavior under different scenario. As regard the earthquakes, a near-fault ground motion from AQK station and a far-fault ground motion from MTR station have been selected and they were both scaled in time according to similitude theory and also scaled in PGA, because they have very different PGA values and without scaling it the results would have been meaningless. Further information about earthquakes will be reported in the next chapter. As regard soil conditions, three different soil condition have been simulated by changing the foundation stiffness; in particular soft soil (4 N/mm), a medium soil (20 N/mm) and hard soil (200 N/mm) have been chosen. Time history results for the all combinations are reported in the following graphs. Related to the mid-span deck displacements, results are:

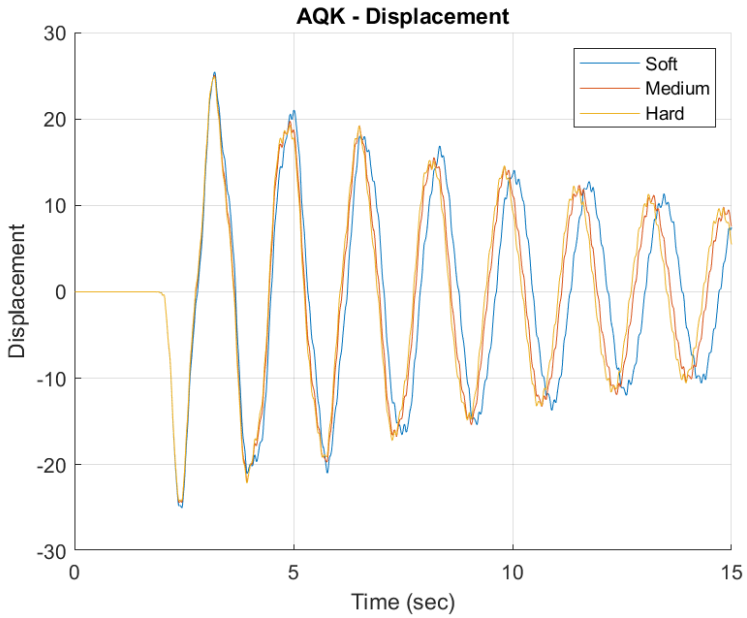

Figure 5.11: AQK Mid-Span Deck Displacement

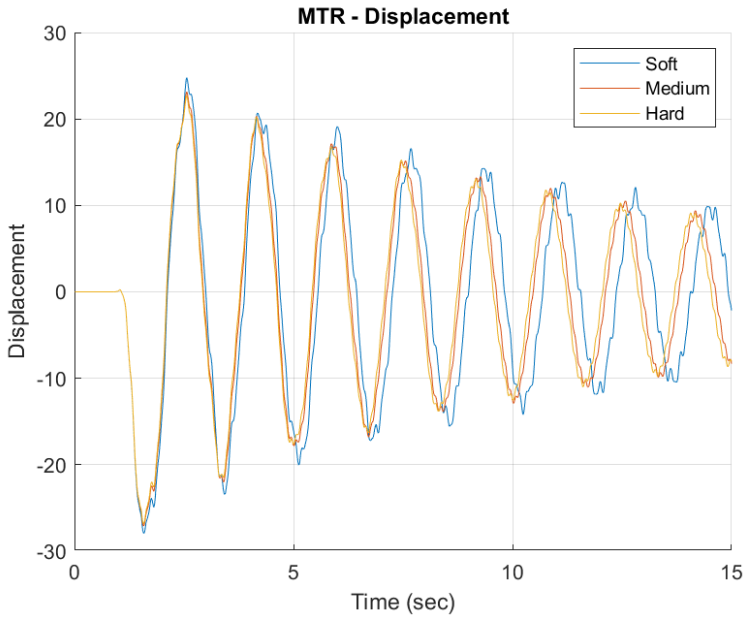

Figure 5.12: MTR Mid-Span Deck Displacement

Showing in the first 7 seconds the earthquake response and then the free-vibration response. As expected, can be noticed how softer soil lead to a higher deck displacements especially in the case of near-fault ground motion. Related to the suspenders response,

results are shown in the following graph for SUS06, the one closest to the tower:

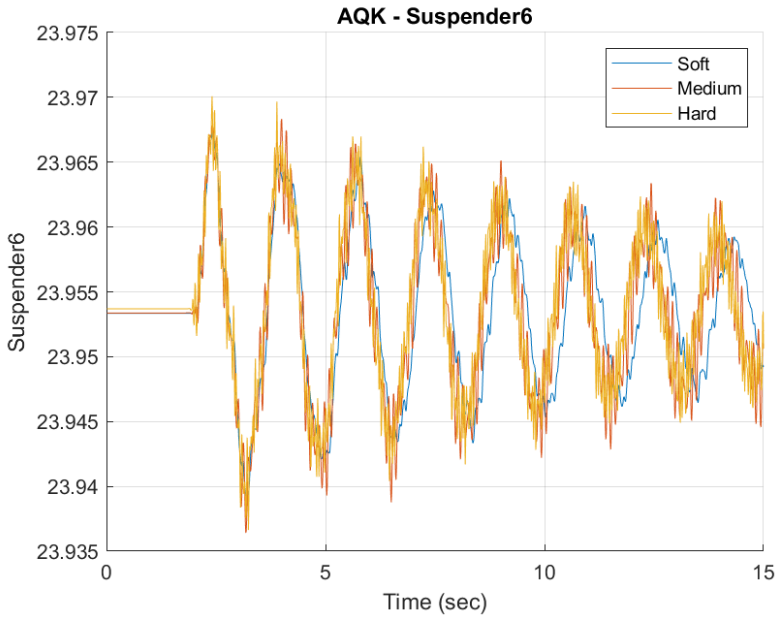

Figure 5.13: AQK - Suspender Tension

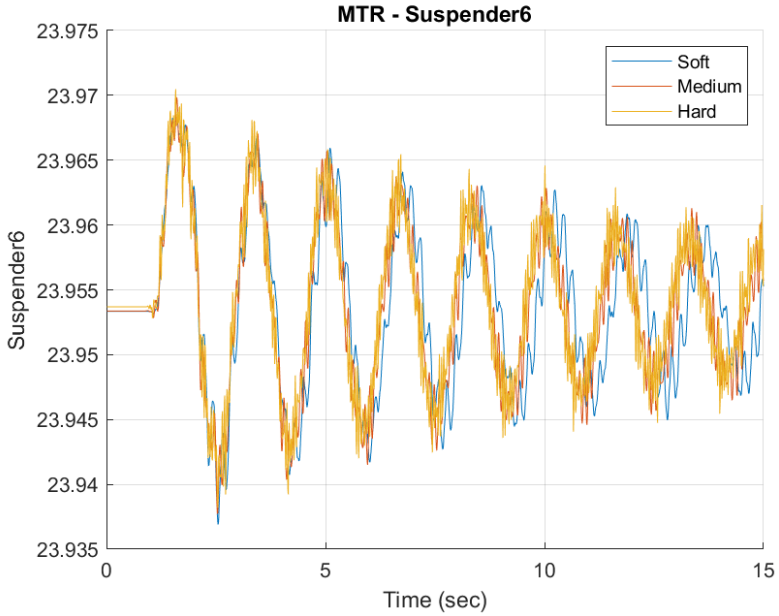

Figure 5.14: MTR - Suspender Tension

Results show that softer foundations dissipate more energy and this lead to a decrease in suspender tension by reducing the stiffness of the soil.

5.1 Experimental Plan

From the conducted DCR analysis, the optimal sensors placements location has been identified, in particular Fiber Bragg Grating (FBG), to measure the tensile force, Linear Variable Differential Transformers (LVDT), to measure the displacement, and shaker, to apply the ground motion, have been installed. In the following figure all these placements are illustrated:

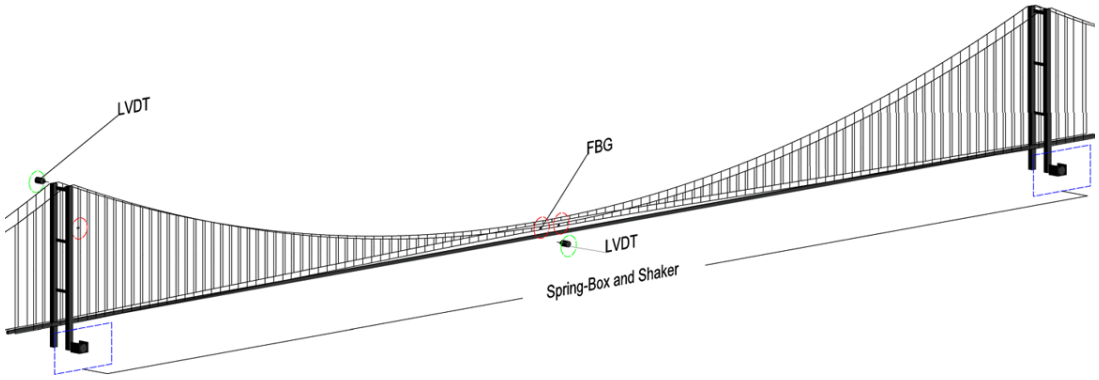

Figure 5.15: Sensors Set-Up

The most critical scenario obtained from numerical findings is related to the sudden removal of suspender SUS59 and for this reason, FBG sensors are placed at suspender SUS58 and SUS60 which are the two adjacents one, to measure the real-time tension response when subjected to ground motion. In addition, SUS06 was also equipped with FBG sensors because is the suspender with the highest tension. As regards the displacements monitoring, LVDT sensors are placed at the mid span and at the top tower, to capture the horizontal displacements during seismic motion. At the base of the tower, both shakers, to apply ground motion, and spring box system, to simulate different soil conditions, have been placed.

5.1.1 Ground Motion

In this section, farther information related to the selection of the input earthquake are provided. In particular the objective was to compare the bridge's seismic response under two different seismic motion specifically a near-fault ground motion and a far-fault ground motion, because these earthquake have a very different nature and a comparison between them could lead to important consideration. Is important to cite the distinction between the two earthquakes and their main characteristics. In general a near-fault earthquake is characterized by high intensity pulses while far-fault earthquake is characterized by longer duration but with lower amplitude. Near fault ground motion has larger velocity pulse, and exposes the structure to high energy in the beginning of the earthquake. The pulses are in general strongly influenced by the orientation of the fault. Therefore near fault earthquakes referred to ground motion recorded in the vicinity of the fault, with a distance non greater than 10 km, characterized by a pulse duration larger than 1.0 s and a peak ground velocity/peak ground acceleration, defined as PGV/PGA, larger than 0.1 s [1]. On the contrary, in far-fault ground motions the impulsive behavior is less pronounced and they are generally composed by a more distributed energy over the time. This lead usually to a less severe damage to the structures. Furthermore, far-fault ground motions

are recorded to greater distances from the fault and they have a lower PGV/PGA value [1]. As consequence, is important to have a distinction between near-fault and far-fault because this can lead to a very different structural response even if the PGA is the same [14].

For this research, the L'Aquila earthquake has been selected from two different station to represent the far fault and the near fault. As regards the near-fault ground motion, AQK station has been selected and it is characterized by a Joyner-Boore distance (R_{jb}) of 0 km, meaning that the station is located above the rupture plane, confirming the near-fault nature of the seismic input. The chosen signal is reported in the figure 5.16.

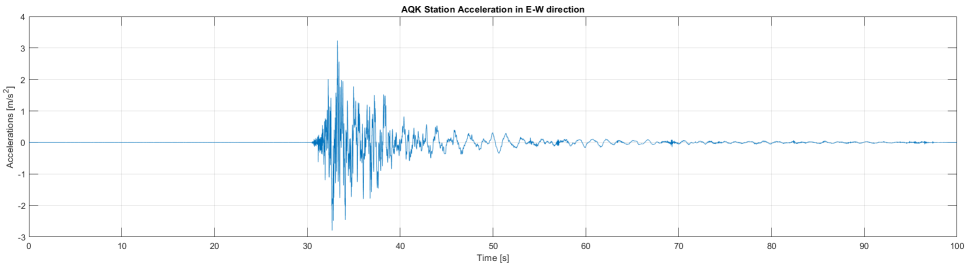

Figure 5.16: AQK Accelerogram Record in E-W Direction

Instead, as regard the far-fault ground motion, the chosen station is the MTR station, which is characterized by a Joyner-Boore distance (R_{jb}) of 16 km from the fault rupture. For this reason can be identified as far-fault earthquake 5.17.

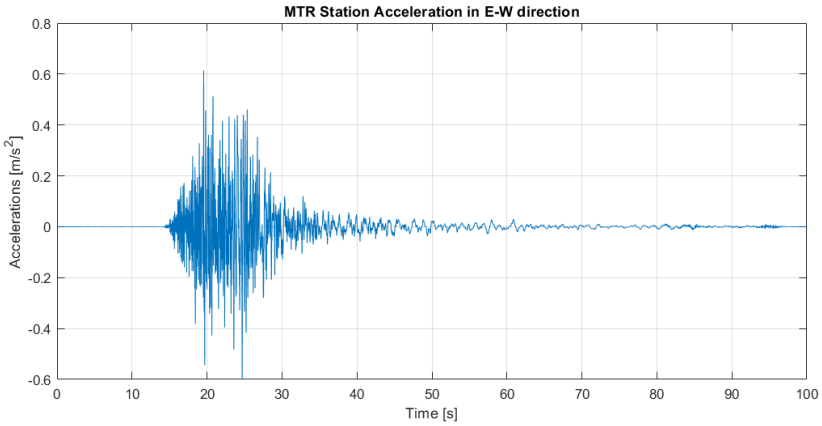

Figure 5.17: MTR Accelerogram Record in E-W Direction

In the following table 5.2, the most important parameters for both selected earthquakes are illustrated:

Earthquake	**Station**	**Type**	**Rjb** [km]	**Epicentral** [km]	**PGA** [cm/s^2]	**PGV** [cm/s]	**PGV/PGA** [s]
L'Aquila	AQK EW	Near-fault	0.0	1.8	346.784	35.798	0.103
L'Aquila	MTR NS	Far-fault	16	23.1	61.371	2.886	0.047

Table 5.2: Ground motion parameters for two stations from the L'Aquila earthquake

Can be noticed how the AQK earthquake has higher velocity pulses and this characteristics can be easily observed in the time history presented in the figure 5.18. In general, near-fault ground motion generates more damage to the structure [2].

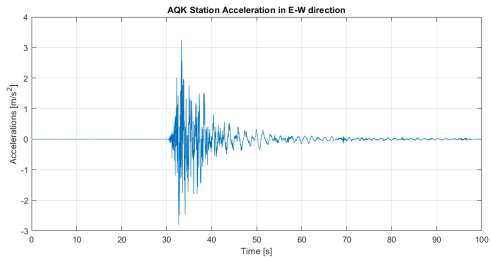

(a) AQK Station Acceleration

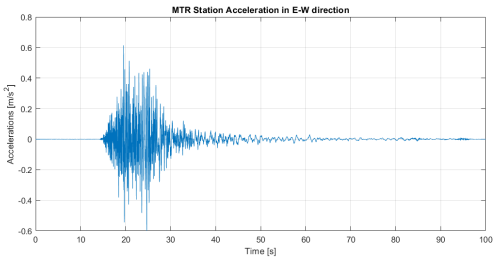

(b) MTR Station Acceleration

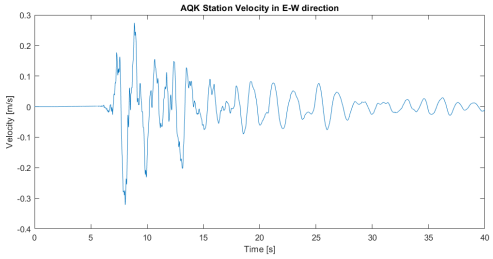

(c) AQK Station Velocity

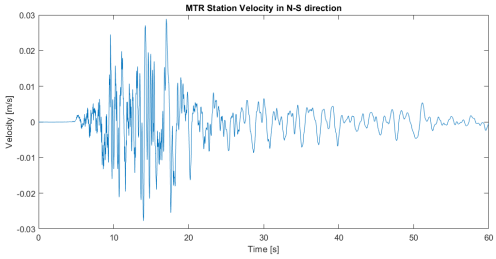

(d) MTR Station Velocity

Figure 5.18: AQK and MTR Acceleration and Velocity

The acceleration response spectra for both earthquakes is illustrated in figures 5.19 and 5.20. Can be noticed how AQK is more impulsive and characterized by shorter but stronger pulses, instead the MTR has a more distributed energy along more frequencies.

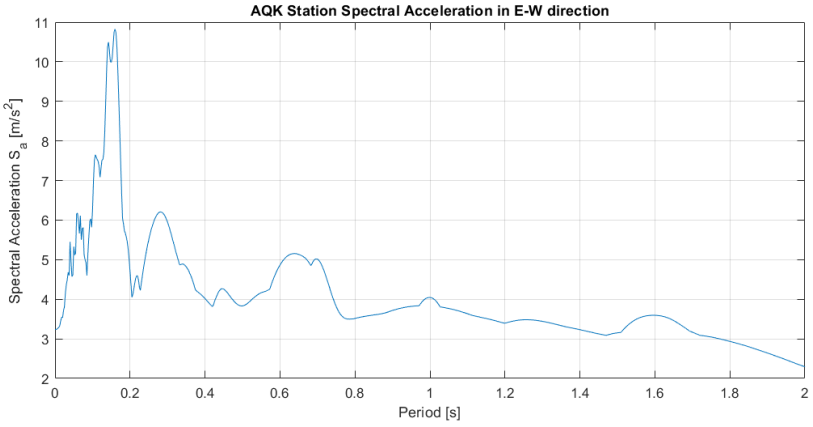

Figure 5.19: AQK Spectral Acceleration

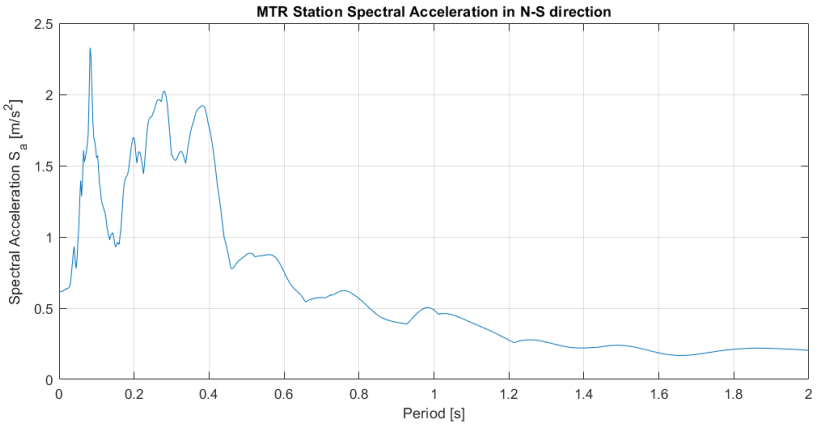

Figure 5.20: MTR Spectral Acceleration

The next step is to scale in time the input ground motion because is important to match the condition provided by similitude theory to ensure the compatibility between the scaled model behavior and the prototype bridge behavior. The time scale factor, having a value of 0.0614 obtained in the similitude theory chapter, has been applied to both earthquakes providing the input signal for the numerical analysis. Results are showed in the following figure 5.21 and 5.22.

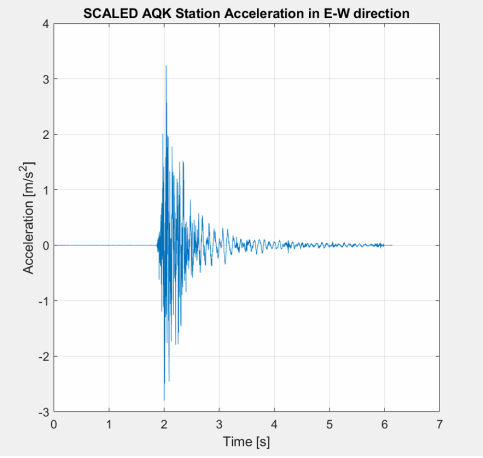

Figure 5.21: AQK Scaled in Time

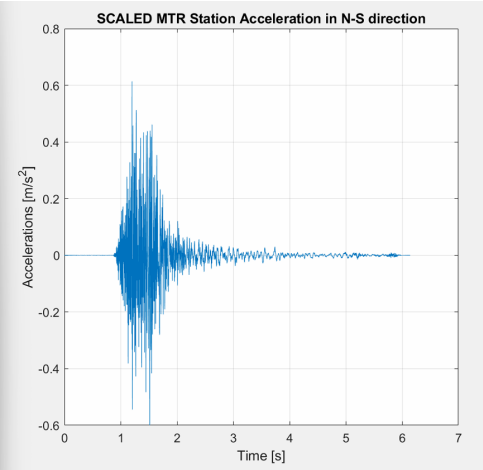

Figure 5.22: MTR Scaled in Time

Some important consideration can be done after the application of the scale factor because can be noticed that having an high geometric scale factor lead to having a high time scale factor resulting in a huge compression in time of the earthquakes implicating a slight loss in the difference between near fault and far fault characteristics. By observing in more detail the two figures 5.18 and figure 5.21, can be noticed the loss in distinction in the two ground motions.

The last step is the scaling in the PGA, the reason behind this choise is because the main objective is to compare both earthquakes focusing on their intrinsic characteristics that depend on the nature of the ground motion. By having a different PGA the two earthquakes are not comparable, therefore PGA value as been set as 0.4 g. This value is assumed as an arbitrary value because in next developments of this research, the experimental analysis should be performed and based on that, starting from a value of 0.1 g and by doing different trial could be possible to identify a real representative PGA value in order to have a notable distinction between the ground motions. In the following figure, hence, the input ground motions applied in Midas Civil for numerical analysis are reported:

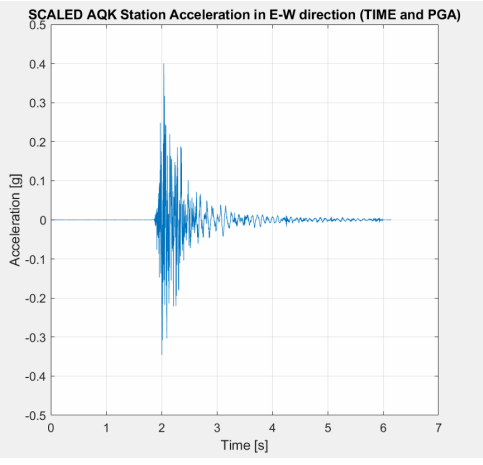

Figure 5.23: AQK Scaled in Time and PGA

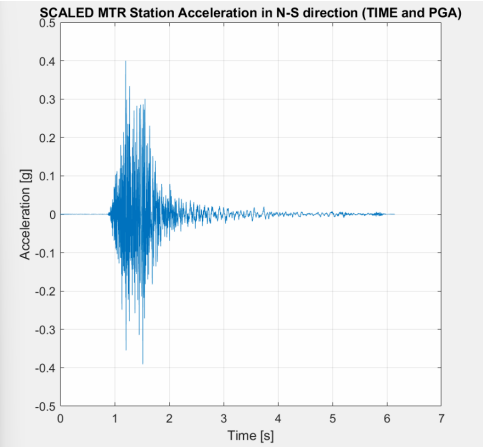

Figure 5.24: MTR Scaled in Time and PGA

5.1.2 Spring-Box System

In this last section all the information related to the designed spring box system used to simulate different soil conditions are reported. In particular, a customized spring box system was designed and implemented to simulate three soil scenarios by changing the spring stiffness [17]. The spring-box system is composed by a steel plate at the base which is equipped with four roll bearings to allow translation, for this reason a translating steel plate is placed above the bearings allowing the later movement when subject to ground motion. As results, the input ground motion is transmitted to the plate which transmits the force to the springs, simulating different soil conditions depending on spring stiffness. In the following figures, detailed pictures showing how the spring-box system is composed, are illustrated:

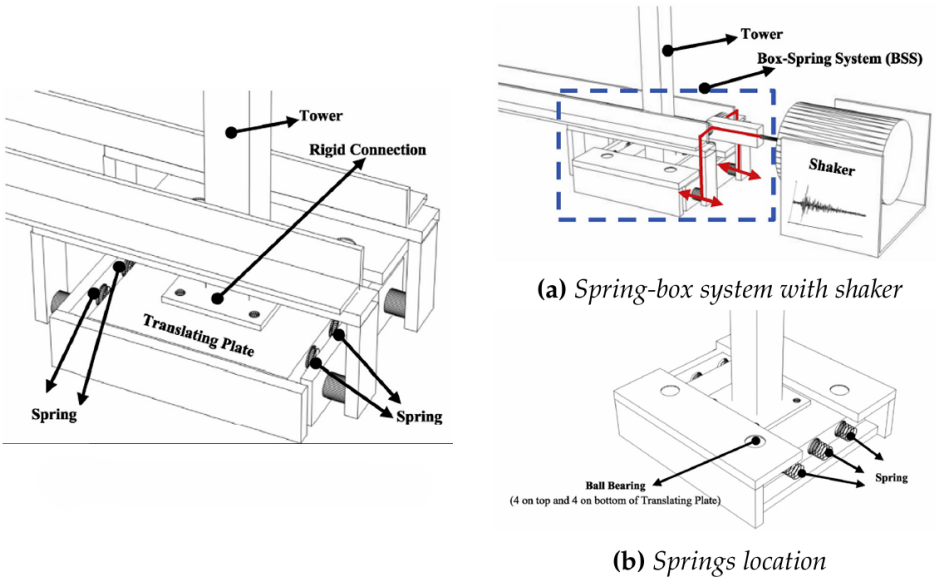

(a) *Spring-box system with shaker*

(b) *Springs location*

Figure 5.25: Spring-Box System

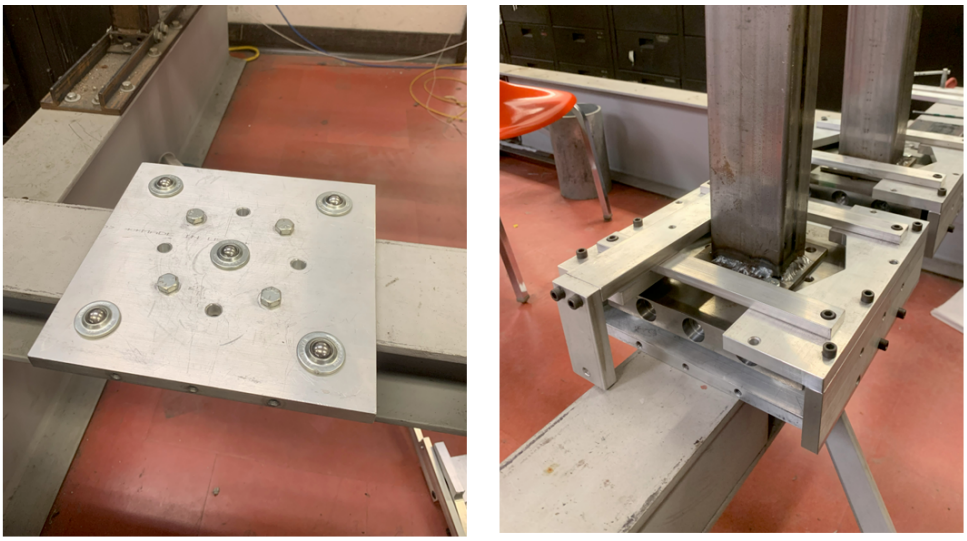

Figure 5.26: Laboratory Spring-Box System

Chapter 6

Conclusion

The main goal of this project, was to design a scaled model of the Messina Strait Bridge in the University of Chicago and to study its dynamic behavior when subjected to ground motion under different soil conditions performing numerical analysis and then experimental analysis for the validation of the results. The first step of this project was scaling the prototype bridge, in particular a geometrical scale factor of 1/265 has been used, according to laboratory size. By applying similitude theory, the scale factors for the physical quantities have been obtained that are used to obtain the perfect similarity, in static and dynamic analysis, between the prototype and the scaled model. In order to design the scaled bridge in the lab, a preliminary FE model using Midas Civil has been created to identify all the elements cross sections useful to reach the target physical quantities. After FE model creation, all the materials used for the realization of the scaled model have been ordered and used in the construction stage phase. Furthermore, a spring-box system has been designed and implemented, costituted by a translating plate on roll bearings, to represent different soil conditions. From numerical analysis, firstly, a DCR analysis has been conducted to identify the best sensors placements and to investigate the behavior of the bridge under seismic motion when subjected to cable loss. In particular, analysis results reveal that the worst damaged scenario is obtained by removing suspender SUS59 and therefore FBG sensors are placed to SUS58, SUS60 and SUS06, to study the seismic response in a damaged scenario. Due to software limitation, the seismic behavior in damaged condition is postponed to experimental analysis, which is still waiting to be completed, as Midas Civil does not support the ground motion application in this specific case. Despite this limitation, numerical analysis revealed that the damage in suspender has a very localized effect, showing how only suspenders in the immediate vicinity of the fractured one are affected, recording a high increse in tension, while the ones farther away are hardly influenced. An other similar consideration is related to the suspenders placed on the opposite side of the fractured one and also in this case, has been noticed how damage does not propagate across the plane. Has been studied how main cable's tension is slightly affected from suspender removal. As regards vertical displacements, cable loss generates a localized increase in deformation only in the area surronding the fractured cable, confirming the strictly localized nature of the phenomena. Furthermore, results reveal that DCR of shorter hangers are generally higher than the longer ones, highlighting their more vulnerable and sensitive nature. As regards the bridge's dynamic behavior in undamaged configuration, three different soil scenarios and two earthquakes have been selected. In particular, the spring box system was adopted to simulate a soft soil, having a stiffness of 4 N/mm, a medium soil, having a stiffness of 20 N/mm and

a hard soil, having a stiffness of 200 N/mm. The chosen earthquake was the L'Aquila earthquake taken from two different stations, in order to compare a near-fault ground motion (AQK station) and a far-fault ground motion (MTR station). Numerical results reveals that softer soil lead to higher deck displacements, especially in the case of near-fault ground motion, when compared to the other cases. Furthermore, has been noticed the effectiveness of the spring-box system in simulating different soil scenarios, showing and highlighting the importance to consider the soil-structure interaction (SSI) in modelling a bridge's seismic response. Findings shows that neglecting SSI could lead to an underestimation of the results compromising the accuracy of the model. This research creates a preliminary contribution for future works and developments in order to better understand the seismic behavior of suspension bridges, in particular the Messina Strait Bridge. The next steps are the validation of the numerical results on the experimental analysis and improving the seismic response by finding a way to perfectly match the static and dynamic similarity. An other aspect that could be improved is the one related to the spring-box system, incresing the representativeness of the soil structure interaction by trying to simulate real soil condition such as composite or layered soil. This could means to involve different springs combination, introducing also vertical springs, or modelling the non-linear behavior of the soil.

Bibliography

[1] Süleyman Adanur, Ahmet Can Altunişik, Alemdar Bayraktar, and Mehmet Akköse. Comparison of near-fault and far-fault ground motion effects on geometrically nonlinear earthquake behavior of suspension bridges. *Natural Hazards*, 64(1):593–614, 2012.

[2] Aybige Akinci, Luca Malagnini, and Fabio Sabetta. Characteristics of the strong ground motions from the 6 april 2009 l'aquila earthquake, italy. *Soil Dynamics and Earthquake Engineering*, 30(5):320–335, 2010.

[3] Maurizio Ponte Alessandro Guerricchio. Aspetti geologici e di stabilità per il ponte sullo stretto di messina. *Giornale di Geologia Applicata 3*, pages 83–90, 2006.

[4] A Balasubramanian. Bridges and their types. *Centre for Advanced Studies in Earth Science, University of Mysore, Mysore, India, Tech. Rep*, (6), 2017.

[5] et al. Brancaleoni F. *The Messina Strait Bridge. A challenge and a Dream.* 2010.

[6] Luigi Callisto, Sebastiano Rampello, and Giulia M.B. Viggiani. Soil–structure interaction for the seismic design of the messina strait bridge. *Soil Dynamics and Earthquake Engineering*, 52:103–115, 2013.

[7] Paolo Clemente. Effects of differential displacements between the ground anchors in suspension bridges. *Infrastructures*, page 19, 2024.

[8] Stretto di Messina S.p.a. Stretto di messina, 2011.

[9] Filippo Gazzola. *Brief History of Suspension Bridges*, pages 1–41. 01 2015.

[10] Tadaki Kawada. *History of the modern suspension bridge. Solving the dilemma between economy and stiffness.* 2010.

[11] Weiwei Lin and Teruhiko Yoda. *Bridge engineering: classifications, design loading, and analysis methods.* Butterworth-Heinemann, 2017.

[12] M.P. Petrangeli. *Costruzione di ponti. Appunti delle lezioni.* ESA, 1988.

[13] Gajanan M. Sabnis, Richard N. White, M. Saeed Mirza, and Harry G. Harris. *Structural modeling and experimental techniques / Gajanan M. Sabnis, Harry G. Harris, Richard N. White, M. Saeed Mirza.* Prentice-Hall civil engineering and engineering mechanics series. Prentice-Hall, Englewood Cliffs, N. J, c1983.

[14] Gökhan Barış Sakcalı, Muhammed Bilal Bağbancı, Yusuf Öztürk, and Çiğdem Meriç Cevahir. Seismic performance of nilüfer hatun bridge pre- and post-restoration under near-fault and far-fault ground motions. *Engineering Failure Analysis*, 177:109677, 2025.

[15] David Barnard Steinman. *A practical treatise on suspension bridges: their design, construction and erection.* Wiley, 1922.

[16] Hongbin Sun, Zhen Sun, and Yongfeng Yao. Hanger replacement and corrosion assessment in a suspension bridge. *Structures*, 58:105501, 2023.

[17] Emad Norouzzadeh Tochaei, Todd Taylor, and Farhad Ansari. Effects of near-field ground motions and soil-structure interaction on dynamic response of a cable-stayed bridge. *Soil Dynamics and Earthquake Engineering*, 133:106115, 2020.

[18] Hongfan Wang, Qian Chen, Anil K. Agrawal, Sherif El-Tawil, Baidurya Bhattacharya, and Waider Wong. Dynamic response and progressive collapse of a long-span suspension bridge induced by suspender loss. *Journal of Structural Engineering*, 148(6):05022001, 2022.

[19] Hongfan Wang, Qian Chen, Anil Kumar Agrawal, Sherif El-Tawil, Baidurya Bhattacharya, and Waider Wong. Performance of a long-span suspension bridge subjected to sudden single suspender loss. *Journal of Bridge Engineering*, 28(11):05023006, 2023.

[20] Wenming Zhang, Genmin Tian, and Yupeng Chen. Evolution of suspension bridge structural systems, design theories, and shape-finding methods: A literature survey. *Journal of Traffic and Transportation Engineering (English Edition)*, 11(2):225–244, 2024.

Figure Sources

Figura 2.1: Fonte: [Lin, Weiwei and Yoda, Teruhiko, *Bridge engineering: classifications, design loading, and analysis methods*, Butterworth-Heinemann, 2017. Pag. 7].
Figura 2.2: Fonte: [Lin, Weiwei and Yoda, Teruhiko, *Bridge engineering: classifications, design loading, and analysis methods*, Butterworth-Heinemann, 2017. Pag. 7].
Figura 2.6: Fonte: [Lin, Weiwei and Yoda, Teruhiko, *Bridge engineering: classifications, design loading, and analysis methods*, Butterworth-Heinemann, 2017. Pag. 22].
Figura 2.8: Fonte: [Lin, Weiwei and Yoda, Teruhiko, *Bridge engineering: classifications, design loading, and analysis methods*, Butterworth-Heinemann, 2017. Pag. 26].
Figura 2.9: Fonte: [Lin, Weiwei and Yoda, Teruhiko, *Bridge engineering: classifications, design loading, and analysis methods*, Butterworth-Heinemann, 2017. Pag. 27].
Figura 2.10: Fonte: [Lin, Weiwei and Yoda, Teruhiko, *Bridge engineering: classifications, design loading, and analysis methods*, Butterworth-Heinemann, 2017. Pag. 29].
Figura 2.11: Fonte: [Lin, Weiwei and Yoda, Teruhiko, *Bridge engineering: classifications, design loading, and analysis methods*, Butterworth-Heinemann, 2017. Pag. 197].
Figura 2.12: Fonte: [Lin, Weiwei and Yoda, Teruhiko, *Bridge engineering: classifications, design loading, and analysis methods*, Butterworth-Heinemann, 2017. Pag. 210].
Figura 2.13: Fonte: [Lin, Weiwei and Yoda, Teruhiko, *Bridge engineering: classifications, design loading, and analysis methods*, Butterworth-Heinemann, 2017. Pag. 210].
Figura 2.14: Fonte: [Lin, Weiwei and Yoda, Teruhiko, *Bridge engineering: classifications, design loading, and analysis methods*, Butterworth-Heinemann, 2017. Pag. 198].
Figura 2.15: Fonte: [Lin, Weiwei and Yoda, Teruhiko, *Bridge engineering: classifications, design loading, and analysis methods*, Butterworth-Heinemann, 2017. Pag. 198].
Figura 2.16: Fonte: [Lin, Weiwei and Yoda, Teruhiko, *Bridge engineering: classifications, design loading, and analysis methods*, Butterworth-Heinemann, 2017. Pag. 198].
Figura 2.17: Fonte: [Lin, Weiwei and Yoda, Teruhiko, *Bridge engineering: classifications, design loading, and analysis methods*, Butterworth-Heinemann, 2017. Pag. 201].
Figura 2.18: Fonte: [Lin, Weiwei and Yoda, Teruhiko, *Bridge engineering: classifications, design loading, and analysis methods*, Butterworth-Heinemann, 2017. Pag. 201].
Figura 2.19: Fonte: [Lin, Weiwei and Yoda, Teruhiko, *Bridge engineering: classifications, design loading, and analysis methods*, Butterworth-Heinemann, 2017. Pag. 201].
Figura 2.20: Fonte: [Lin, Weiwei and Yoda, Teruhiko, *Bridge engineering: classifications, design loading, and analysis methods*, Butterworth-Heinemann, 2017. Pag. 201].
Figura 2.21: Fonte: [Lin, Weiwei and Yoda, Teruhiko, *Bridge engineering: classifications, design loading, and analysis methods*, Butterworth-Heinemann, 2017. Pag. 201].
Figura 2.22: Fonte: [Lin, Weiwei and Yoda, Teruhiko, *Bridge engineering: classifications, design loading, and analysis methods*, Butterworth-Heinemann, 2017. Pag. 202].
Figura 2.23: Fonte: [Lin, Weiwei and Yoda, Teruhiko, *Bridge engineering: classifications, design loading, and analysis methods*, Butterworth-Heinemann, 2017. Pag. 202].
Figura 2.24: Fonte: [Lin, Weiwei and Yoda, Teruhiko, *Bridge engineering: classifications,*

design loading, and analysis methods, Butterworth-Heinemann, 2017. Pag. 208].
Figura 2.25: Fonte: [Lin, Weiwei and Yoda, Teruhiko, *Bridge engineering: classifications, design loading, and analysis methods*, Butterworth-Heinemann, 2017. Pag. 207].

Figura 3.1: Fonte: [*https://strettodimessina.it/web/*].
Figura 3.2: Fonte: [*https://strettodimessina.it/web/*].
Figura 3.3: Fonte: [*https://strettodimessina.it/web/*].
Figura 3.4: Fonte: [*https://strettodimessina.it/web/*].
Figura 3.5: Fonte: [*https://strettodimessina.it/web/*].
Figura 3.6: Fonte: [*https://strettodimessina.it/web/*].
Figura 3.7: Fonte: [*https://strettodimessina.it/web/*].
Figura 3.8: Fonte: [*https://strettodimessina.it/web/*].
Figura 3.14: Fonte: [*https://strettodimessina.it/web/*].
Figura 3.15: Fonte: [*https://strettodimessina.it/web/*].
Figura 3.16: Fonte: [*https://strettodimessina.it/web/*].
Figura 3.17: Fonte: [*https://strettodimessina.it/web/*].
Figura 3.18: Fonte: [*https://strettodimessina.it/web/*].
Figura 3.19: Fonte: [*https://strettodimessina.it/web/*].
Figura 3.9: Fonte: [*https://strettodimessina.it/web/*].
Figura 3.10: Fonte: [*https://strettodimessina.it/web/*].
Figura 3.11: Fonte: [*https://strettodimessina.it/web/*].
Figura 3.12: Fonte: [*https://strettodimessina.it/web/*].
Figura 3.13: Fonte: [*https://strettodimessina.it/web/*].

Figura 4.3: Fonte: [*https://strettodimessina.it/web/*].